THE EVALUATION OF POLARIZATION PARAMETERS AS QUALITY PREDICTORS FOR ZINC ELECTROPLATED FROM ACIDIC SULPHATE SOLUTIONS

By

ELLEN CHIYANGWA

Supervisor: Prof RF Sandenbergh

A dissertation submitted in partial fulfilment of the requirements for the degree of

MASTER OF APPLIED SCIENCES (METALLURGY)

Department of Material Science and Metallurgical Engineering

FACULTY OF ENGINEERING, BUILT ENVIRONMENT AND INFORMATION TECHNOLOGY, UNIVERSITY OF PRETORIA, SOUTH AFRICA

JULY 2015

ACKNOWLEDGEMENTS

My profound gratitude goes to my supervisor Professor Sandenbergh. His constructive criticism, expertise and advice were unquantifiable in the course of the research.

My family, colleagues and friends are equally appreciated for their encouragement and push all the way.

TABLE OF CONTENTS

LIST OF TABLES

LIST OF FIGURES

SYNOPSIS

Successful commercial electrowinning and refining of metals typically requires the optimization of the electrolyte composition and operating parameters to produce high quality compact electroplated metal. The prediction of the structure and morphology of the plated metal from the operating parameters remains a challenge. The aim of this work was to develop a reliable galvanodynamic technique to measure nucleation and plating potentials that was specifically applicable to the plating of zinc from sulphate electrolytes, with which plant operation may be controlled and optimized. The work was focussed on determining whether there would exist a definite unique or range of values for both the nucleation and plating potentials for which it would be possible to obtain high quality zinc electrodeposits repeatably. Such a tool could be modelled and be particularly useful in plant situations to suggest remedies for process upsets and development.

In the current study a repeatable and reliable galvanodynamic polarization technique using two scan rates was developed to perform the polarization measurements. The values were used to predict the nature and morphological characteristics of the metal plated from the respective acidic aqueous zinc sulphate electrolytes

The developed galvanodynamic technique was found to be an effective and reliable technique to measure nucleation and plating potentials systematically and repeatably. The results indicated that nucleation and plating potentials could be obtained with reasonable repeatability of ±3mV. These potentials provided useful data and information on the electrowinning processes and the effect of changes in parameters and conditions of zinc deposition on the morphology. The repeatability and relevance of the potential measurements were strongly dependent on strict adherence to consistency in electrode preparation procedures, electrolyte preparation and control of experimental conditions. .

The relationship between initial nucleation of zinc on an inert aluminium substrate and further growth provided a useful framework for relating the physical changes in the structure of electrodeposits. The difference between the nucleation and plating potentials was observed to be an indicator of the type, quality and characteristics of the deposits formed, and could be used to identify a unique region which is considered to be the region in which the most desirable quality deposit will be obtained. However the idea suggested by Adcock et al. (2002), that nucleation is favoured over growth if the plating potential is more negative than the nucleation potential ΔE, and should therefore result in unoriented dispersion (UD) type deposits turned out to be only partly so

with such deposits rather obtained for ΔE values around zero and with field oriented texture (FT) and basis reproduction (BR) type deposits obtained at more positive as well as negative values.

The effect of temperature on the plating characteristics was not significant. This may have been attributed to the influence of hydrogen ion reduction on the potential whereby a substantial current flow and a shift of potentials to positive values is observed, but not necessarily due to zinc plating. Higher temperatures showed a considerable reduction in current efficiency which is a consequence of high rates of hydrogen reduction. This indicated that the approach to characterise zinc plating by polarization characteristics would probably not be valid for conditions where significant rates of hydrogen ion reduction occur.

The study indicated that grain refiners influence the nucleation process while levellers change the growth process. The difference between the plating and nucleation potentials ΔE was found to be an indicator for identifying and predicting grain refinement but not as much as in the case with levelling. This limits the usefulness of the two dimensional representation of the polarization parameters, such as suggested by Adcock, for the evaluation of additives for zinc electrowinning from sulphate electrolytes.

Keywords

Electrocrystallization, polarization, morphology, electrowinning, zinc

1 INTRODUCTION

1.1 General background

In conventional zinc electrowinning cells the aim is to reduce dissolved zinc to metallic zinc at the cathode in an electrowinning cell. To achieve this, an electric current is passed through typically an aluminium cathode, an electrolyte of acidic aqueous zinc sulphate and a silver-alloyed lead anode. The cathodic reaction is primarily the electrodeposition of zinc. The evolution of hydrogen gas also takes place at the cathode as a competing side reaction which reduces the cathodic current efficiency of the plating process. The anodic reaction is primarily the decomposition of water into hydrogen ions and oxygen with the oxidation of manganese present in the electrolyte also playing a minor role. The efficient operation of an industrial electrowinning process also requires the electroplated metal to be relatively smooth and mechanically tough. Literature indicates that many parameters impact on the quality of the metal produced and the overall efficiency of the process. The challenge is to solve this multivariable optimization problem for each particular application.

1.2 Challenges in controlling and predicting the electrodeposit structure

Successful commercial electrowinning and refining of metals typically requires the optimization of the electrolyte composition and operating parameters to produce high quality compact electroplated metal cost effectively. However, the structure and morphology of the electroplated metal are dependent on interrelated variables such as the composition and surface condition of the electrode, the metal ion concentration, additives, surface tension, viscosity, the operating current density, temperature and impurities present in the electrolyte. In addition, these variables are also time dependent as some impurities and additives accumulate over time on the surface of the cathode to typically limit the economically viable time of plating. This makes the prediction and control of the plated metal structure and morphology a challenge.

1.3 Use of the overpotential as a control tool for electrocrystallization

The control of electrodeposition processes in zinc electrowinning tankhouses to achieve a desired structure and morphology is possible if the electrocrystallization process can be controlled. This can be achieved through the control of the nucleation and growth processes. Nucleation or growth of a solid on the electrode substrate is achieved by polarizing the electrode such that the electrolyte

solution in contact with the electrode becomes supersaturated with the metal species in solution as described using the Nernst equation (Paunovic and Schlesinger, 2006). The kinetics of the plating process can be conveniently described in terms of the rate, typically expressed in terms of current density, achieved at a certain overpotential, i.e. the induced potential relative to the reversible potential for the half cell.

It is of fundamental and technological importance to express electrodeposition by means of physical quantities that can be measured and controlled. The growth rate is indicated by the current density, and the supersaturation can be manipulated by changing the potential of the electrode such that the electronation of the metal species in solution is favoured to such an extent that significant charge transfer occurs and metal is plated. The formation of a new phase requires additional surface energy that is supplied to the electrode in the form of an externally applied overpotential.

A ‘nucleation overpotential’ may be identified for a certain set of experimental parameters at which the formation and survival of nuclei become viable, as indicated by the flow of current in for example a potentiodynamic experiment. Growth of nuclei typically requires less energy as the surface area to volume ratio of the precipitate decreases with the size of the crystal (Budevski et al., 2000). Growth is therefore typically favoured following the initiation of new nuclei, and if uncontrolled, it would result in uneven and irregular deposits which are typically nodular, dendritic or even powdery. This is not desired in commercial production.

The production of quality electrodeposits therefore requires that the rates of the nucleation and growth be carefully balanced. Considering all nucleation sites to require equal energy for nucleation is an oversimplification as a hierarchy of sites with different energies typically exists on metal surfaces. Those having the most neighbours, such as for instance an atomic hole or a corner on a ledge offer the most attractive sites for nucleation. Nucleation may also be statistically favoured at other sites or further additions at that site promoting growth. The nucleated atom may diffuse away to the energetically most favoured sites, then determining the structure of the deposit formed. However, it can be expected that in the case of industrial electrowinning the rates of plating are relatively high and it can be expected that surface diffusion will play a comparatively minor role in determining the nature of the deposit.

It is generally agreed that electrodeposited metals are crystalline and that the microstructure and morphology depends on the relative rates of nucleation and growth. Optimum deposit morphology can be obtained by control of the nucleation stage, the growth mode and the coalescence of the metal ion clusters at the commencement of deposit formation. The relative rates between growth

and nucleation determines the grain size of the deposit. Each nucleating cluster eventually becomes a grain in the final product, if surface diffusion and the addition of atoms to ledges play an insignificant role. An increase in the nucleation rate during deposition increases the number of grains. When this is combined with low growth rates there is more time for further nucleation to take place in the parent phase that lies between slowly growing particles. An increasing nucleation rate combined with a decreasing growth rate should result in finer crystal grains in the deposit. However, if the finer grained precipitates agglomerate they may occlude more electrolyte than a solid crystal implying that a compact continuous three dimensional nucleation and growth mode should preferably be maintained throughout plating. However, at too high current densities the viable nucleus becomes very small and undesirable powdery deposits with high surface to volume ratios and poor adherence form (Winand, 1991).

The challenge in electrowinning is to control plating conditions such that continuous nucleation and growth occur to produce fine and compact deposits. This is achieved for example by the addition of additives to the electrolyte to inhibit mainly growth, and the choice of current density used. The choice of additives is rather difficult because nucleation and growth do not occur independently but actually overlap such that their mechanisms are not well understood.

The main focus of this work is to utilise the concept of relative rates of nucleation and growth as processes dependent on the available energy provided to predict and control electrodeposition processes in zinc electrowinning. It is suggested that this be done by measuring the overpotentials required for nucleation and growth, and to use these as parameters to optimize the electrolyte and plating conditions to obtain desirable deposits in the most economical way.

2 LITERATURE REVIEW

2.1 Historical review of methods used to monitor electrolytes

Initial efforts to predict the effects of electrolyte composition and operating parameters on the electrowinning of zinc focussed on the use of potentiodynamic polarization measurements, such as cyclic voltammetry to determine the effects of impurities and additives on what was defined as the overpotential. This was a potential at which plating initiated as indicated by a sudden increase in the cathodic current. Examples of this approach are the work reported by Kerby et al. (1977), Mackinnon and Brannen (1977) and Warren (1985) which is summarised in figure 2.1. Potentiodynamic polarization experiments, in which the potential was varied in a linear manner starting from an initial value to the pre-defined limiting value where the direction of the potential scan was reversed, and the same potential window scanned in the opposite direction, were typically used. The metal plated during the forward scan would then be oxidised on the reverse scan and the charge required for that used to calculate the current efficiency

The initial interest was in the overpotential required to nucleate zinc from zinc containing sulphuric acid electrolytes on an inert electrode such as aluminium, which naturally forms a passive layer of hydrated aluminium oxide. It was for instance shown that the nucleation potential moved to more positive potentials in the presence of an impurity such as antimony, added as Sb^{3+} or Sb^{5+} to the electrolyte, and that this trend could be reversed by the further addition of glue to the electrolyte. As this also reversed the negative influence of antimony on the plating efficiency in practical circuits, and indeed increased the current efficiencies to levels higher than that achieved without additions, it was suggested for use as a method to guide the optimal make-up of the electrolyte. However, it was found that the technique was very sensitive to other impurities as well, and required a rather elaborate experimental set-up to obtain reliable results. This technique could also not predict the nature of the deposit formed as the ‘plating potential’ is a rather lumped parameter that does not characterise the fundamental processes that determine the nature of the precipitate, as will be further discussed in the next sections.

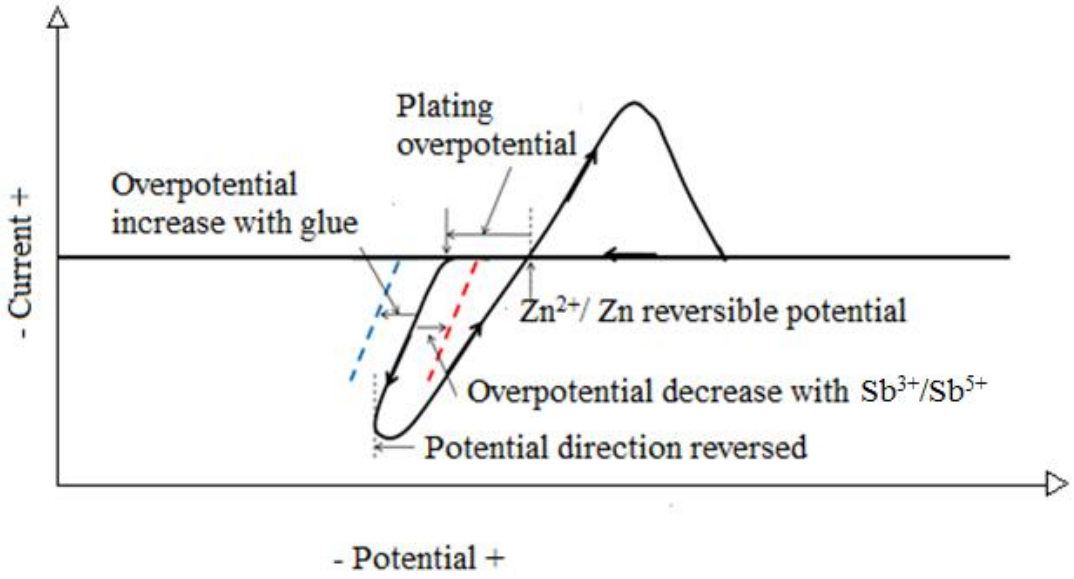

Figure 2.1. Schematic potentiodynamic polarization diagram illustrating the effect of glue and antimony additions to a sulphate electrolyte on the overpotential required for zinc plating on passive aluminium (After Kerby et al., 1977).

The optimization of the additives used in the zinc cell house to achieve good quality cathodes remains a challenge. The deposit is considered to be of poor quality when it is rough, nodular and brittle. Nodules often cause short circuits when they grow into the anodes with a resultant reduction in current efficiency and possible entrapment of anode slimes into the cathode reducing cathode purity. Research efforts are typically focussed on the determination of the appropriate concentration of the additives, monitoring and control of the actual additives' activity in the electrolyte as well as the use of alternative additives. The most common additives currently used in the electrowinning of zinc are levellers and grain refiners. Levelling in this context refers to a general reduction in surface macro roughness by promoting electrodeposition rates that are relatively faster in small recesses and relatively slower on small protrusions. A good grain refiner basically produces finer crystallites.

Additives also affect the kinetics of deposition by complexing with metal ions or shielding adsorption sites on the cathode surface. The additive molecules may be adsorbed, desorbed or incorporated in the deposit (Paunovic et al., 2006). The inhibitor is needed to slow down the rate of electrocrystallization but the challenge is that it has to be destroyed or incorporated into the deposit to limit the inhibition, which will tend to increase over time, while there must also be some possibility to reactivate the process by means of nucleation.

Typically in the case for zinc electrowinning, a combination of several addition agents is necessary for optimal control of zinc electrocrystallization. Overall control of the electrodeposition process is

thus achieved by the use of two counteractive regulators. Improper concentrations or concentration ratios of the additives can lead to cathode nodulation or a general increase in surface macro roughness. The optimum concentration and concentration ratio of the inhibitor depends on the electrolysis parameters, mainly current density, anode composition, temperature and hydrodynamic behaviour of the electrolyte. These parameters often vary considerably over the duration of the electrolysis cycle and a system for monitoring of actual inhibition would be of benefit.

Most research on the classification, control, and optimization of levellers and grain refiners has been empirical with their behaviour and synergistic interactions in terms of inhibition mechanisms not well understood. Some attempts have been made to establish a relationship between the nature and chemical structure of addition agents and the nature of plated metal deposits. However, the correlations have found limited application as they are typically very specific and based on empirical observations. Some correlations have been developed to predict polarization properties in terms of the structure of organic compounds, e.g. for lead with compounds such as flavone as levelling agents, with strong polarization properties being attributed to the presence of the hydroxyl group in strong proximity to the ketonic group (Kerby and Jackson, 1978). However, compounds from the same molecular group, e.g. p-benzoquinone and anthraquinone, both quinones, have no levelling effect in lead electrorefining, while another quinone, naphtho-quinone is an efficient levelling agent (Oniciu and Muresan, 1991). It is thus clear that predicting the effect of additives on metal plating would require more than just the classification into molecularly similar groups.

It is evident that existing theories to explain the levelling and grain refinement of additives do not satisfactorily explain their mode of action for proper classification and optimisation. Electrochemical measurement techniques such as potentiodynamic polarization (Jin and Ghali, 2001), cyclic voltammetry (Kerby et al., 1977), current transients, and the galvanostatic method (Jin and Ghali, 2001), have been used to identify efficient levelling and grain refinement agents, based on the strong influence of additives on polarization behaviour. A continuous electrolyte quality monitor (CEQM) was developed by Kerby et al. (1977) for the monitoring of additive efficiency in industrial tank houses. It measured the nucleation overpotential generated upon applying a low current to an aluminium foil strip moving through the electrolyte. The measurement was taken at some current density used for conventional plating and at a certain critical strip speed. A technique based on the independent measurement of nucleation and plating overpotentials was further developed to maintain optimum levelling additions during the electrorefining of lead, called the dual channel quality monitor (Kerby, 1984). The continuous electrolyte monitoring techniques were quite involved since they required simultaneous monitoring of two moving wires.

Among the available techniques, the galvanostatic technique is attractive as it can be used to rapidly evaluate the additive's performance during electrodeposition under a controlled current density. Lafront et al. (2002) used a galvanostatic technique to predict the tendency for nodule formation during copper electrodeposition by evaluating the initial cathode potential and the presence of a cathodic polarization peak on the potential-time curves. However, a comprehensive knowledge of the additive's behaviour at various electrolysis parameters is a prerequisite to gain significant benefit from such measurement systems. Sometimes more than one peak is observed during a single scan making it difficult to decipher which peak is associated with what reaction. The technique is also dependent on the current density used.

Some attempts have been made to measure the crystallization overpotential as a method to predict and control the morphological outcome of electrodeposits. The driving force required for electrodeposition can conceptually be separated into five additive terms, namely, the charge transfer overpotential η_t, the diffusion overpotential η_d, the reaction overpotential η_r, the crystallization overpotential η_c, and the resistance overpotential η_Ω , which may be present due to strong specific adsorption as a dense film of inhibitor at the surface of the metal (Winand, 1994), i.e.

$$\eta = \eta_t + \eta_d + \eta_r + \eta_c + \eta_\Omega \qquad 2.1$$

The driving force for the electrocrystallization process itself is the crystallization overpotential. A measure of the value of this overpotential has been obtained using chronoamperometry and pulse plating which have been used for routine preparation of metal nanoparticles with a very narrow size distribution and also for compact metal films (Saber et al., 2003; Kalantary and Gabe, 1993; Liu et al., 2001). The technique allows for the formation of a large number of metal clusters during the first short pulse at $\eta_1 >> \eta_{critical}$ to measure the nucleation overpotential, followed by polarization at a much lower cathodic overpotential $\eta_2 << \eta_{critical}$ to measure the plating overpotential, as illustrated in figure 2.2. It is, however, difficult to up front estimate suitable limits for the chronoamperometric experiments. Such measurements are also further complicated by the inclusion of the IR-drop between the reference electrode and the working electrode, as well as the change in surface area with time, which effectively changes the current density with time.

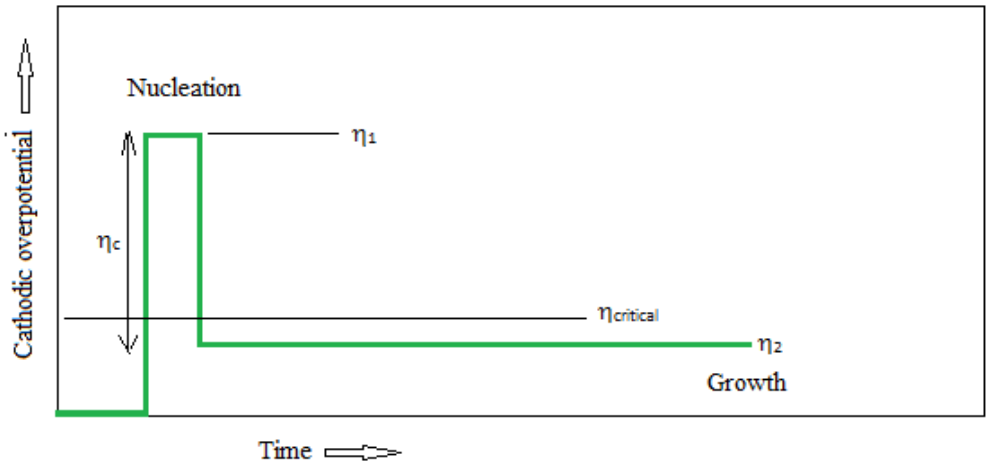

Figure 2.2. Schematic representation of the double pulse polarization routine for preparation of metal nanoparticles and compact metal deposits (After Staikov, 2007).

More recently Adcock et al. (2002) developed a stepped galvanostatic polarization technique to measure the crystallization potential by measuring nucleation and plating potentials reliably and repeatably. This was in an attempt to better characterise the influence of impurities and additives used in zinc electrowinning. The theoretical basis and application of this technique will be further explored in the following sections.

2.2 An overview of electrodeposition processes and process control

Optimal control of electrocrystallization processes should ideally be based on an indepth comprehension of the electrodeposition processes and their relationship with the overpotential at the atomic level. Nucleation and growth of the first metallic nuclei formed on the initial substrate are critical aspects determining the physiochemical properties of the deposited materials. This section discusses the basic processes involved in electrodeposition and the challenges involved in controlling nucleation and growth processes. The practical approaches that have been developed to control and predict the structure of electrodeposits, including their contributions and shortcomings, are also discussed.

2.2.1 Electrodeposition

2.2.1.1 Electrocrystallization

The overall reaction process for the electrocrystallization of an ion in solution onto an electrode involves the mass transport from the bulk of the solution to the outer edge of the electric double layer, followed by the desolvation and movement of the ion to the metal surface through the potential gradient, and finally the discharge of the ion by electron transfer from the electrode to form an adatom on the surface of the metal. A crystal may then form there or the adatoms may move by surface diffusion to low energy sites, such as terraces, steps and kinks, where the atom is then incorporated into the existing metal lattice, as illustrated in figure 2.3. Successive incorporation of adatoms at these sites results in nucleation which can occur instantaneously or progressively. Growth of the nuclei can occur on existing precipitates in one dimensional (1D), two dimensional (2D) or on new sites as three dimensional (3D) directions (Paunovic and Schlesinger, 2006).

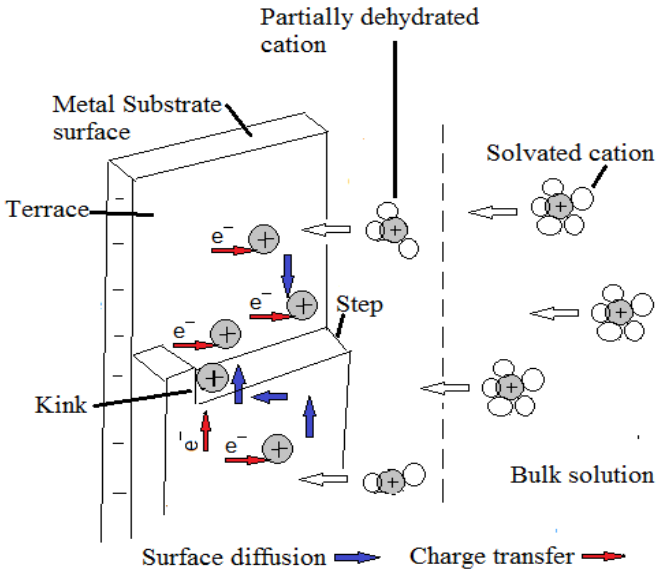

Figure 2.3. Steps involved in electrocrystallization (After Paunovic and Schlesinger, 2006).

2.2.1.2 Control of electrocrystallization

Nucleation is an important phenomenon which plays a fundamental role in crystal growth, especially in electrodeposition. Any phase formation such as the electrocrystallization of a metal on an inert (foreign) substrate begins with nucleation of the new phase. The energy balance for the

nucleation process involves the external energy needed to either create the additional surface of say an adatom or a two or three dimensional cluster on a crystal terrace, with the electrical energy being made available for the movement of the ion through the potential gradient and its discharge on the surface of the electrode. As the surface area per unit volume decreases with the number of atoms in a cluster while the Gibbs free energy contribution is proportional to its volume, there will be a critical size of cluster that will be energetically favourable for a certain potential gradient. The critical size decreases as the polarization of the electrode is increased. The overpotential required for crystallization is thus a function of the type of precipitation site. This effect may be illustrated by considering the energy balance for a two dimensional circular deposit on a crystal terrace of N atoms with an area of s per atom requiring a charge of ze to be reduced with an edge energy per unit length ε (Bockris et al., 2000)

$$\Delta G = -Nze\eta_c + 2\varepsilon(\pi sN)^{0.5} \qquad 2.2$$

The number of atoms N_{crit} and ΔG_{crit} where $d\Delta G/dN = 0$ is then given by:

$$N_{crit} = \pi\varepsilon^2 s/ (ze\eta_c)^2 \qquad 2.3$$

$$\Delta G_{crit} = \pi\varepsilon^2 s/ (ze\eta_c) \qquad 2.4$$

It follows from these equations that the critical number of atoms required for a stable cluster decreases as the overpotential increases but increases as the surface energy required increases. As could be expected in other words, a small critical cluster size is required at higher overpotentials as the energy available from polarization is higher.

The electrical energy required for electrocrystallization will depend on the particular incorporation site, such as those illustrated in figure 2.4.

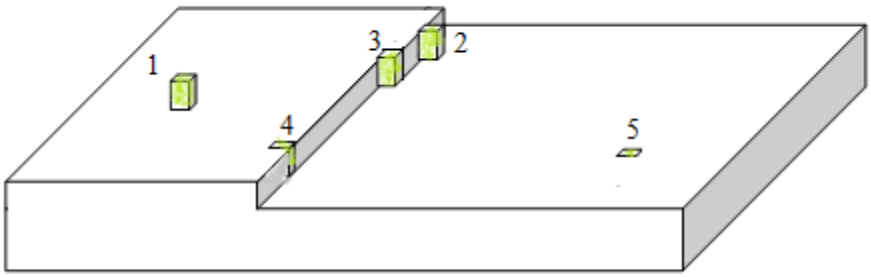

Figure 2.4. Types of positions available for metal deposition. The numbers indicate the number of saturated bonds formed by the precipitated ion for each site (After Winand, 1992).

Due to the short range of interatomic forces the incorporation site which offers most neighbours or saturated bonds will be energetically most favourable. Such sites are typically small in number and only dominant at very low overpotentials, while if abundant external energy is available, such as at high overpotentials, the number of atoms required to form stable three dimensional clusters decreases significantly and will probably be the dominant mode for the electrodeposition of metal. Following the work of Nichols and Kolb (1991), at lower overpotentials, i.e. lower supersaturation, metal deposition exclusively begins at surface imperfections with the preferred site being a kink site. This is indicated by a schematic illustration in figure 2.5 showing how copper was deposited on a single crystal gold substrate with a solution containing a low concentration of copper. The deposition and dissolution in the very initial stages was observed by STM (Scanning Tunnelling Microscopy). The area of the surface was well defined providing a smooth terrace with clearly resolved atomic steps. At the application of an initial potential of +33 mV vs. Cu/Cu^{2+} the gold surface was covered by a monolayer of underpotentially deposited copper. When the potential was stepped into the bulk deposition regime the nucleation and growth of copper was clearly seen to occur exclusively at the monoatomic high steps as schematically indicated in figure 2.5 (b) and (c). The copper clusters which grew in a 3D fashion deposited on the surface defects with a considerable amount of copper being accumulated at the step edges while the flat terraces barely supported plating. It was also observed that curvy steps are more effective than straight steps in terms of providing nucleation centres due to the key role of kink sites.

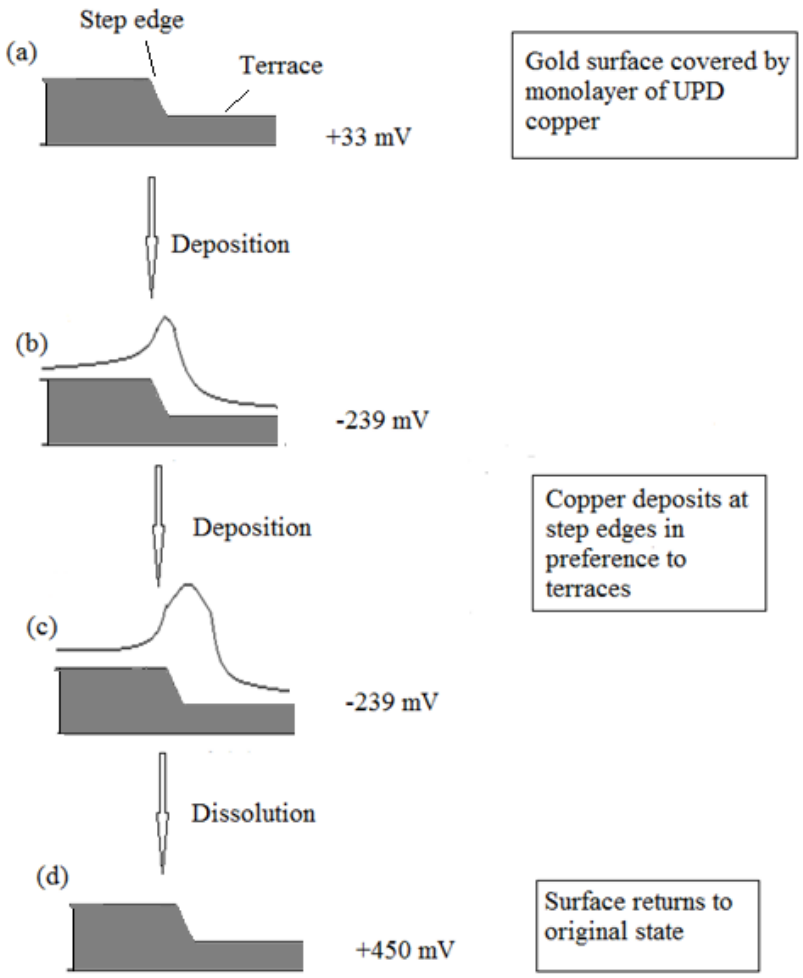

Figure 2.5. Schematic diagram of the preferential plating of copper at the step between terraces on a gold surface (After Nichols and Kolb, 1991).

It can therefore be concluded that substrate surface imperfections and inhomogeneities affect primary nucleation. They strongly influence the local mechanism of the crystallization process and the resulting surface morphology. This significantly complicates the reproducibility and interpretation of experimental results that involve measurement of potentials during the initial stages of nucleation. Therefore the reproducible preparation of a smooth electrode surface is extremely important for the repeatable estimation of kinetic parameters. Other factors that affect the control, quality and prediction of electrodeposits, specifically for zinc in acid sulphate electrolytes are discussed in the following sections.

2.2.1.3 The role of impurities in zinc electrodeposition

The zinc electrowinning process is very sensitive to the presence of impurities. Mackinnon et al. (1987) studied impurity effects on the current efficiency, zinc deposit morphology and orientation, and the polarization characteristics for an aqueous electrolyte containing 55 gL^{-1} zinc, 150 gL^{-1} H_2SO_4 at 35 °C at a current density of 430 Am^{-2}. The effects of various impurities on 1-hour zinc deposits indicated four distinct morphological types with preferred zinc orientations defined by the angle at which the basal plane was aligned to the aluminium cathode, as indicated in table 2.1.

Table 2.1. Zinc deposit morphologies with corresponding preferred orientations, associated impurities and current efficiency (After Mackinnon et al., 1987).

Morphology type	Zn platelet alignment to Al substrate	Preferred orientation*	Associated impurities	Current efficiency
Basal	$0 - 30^0$	(002), (103), (102)	Sb, Se, Te, As(V), Bi, low concentration of Sn	Very low
Intermediate	$30 - 70^0$	(114), (112), (102)	Co, Ni, Cu, Ga, Ge, As(III), Cd and In	High
Triangular	$\sim 70^0$	(101)	Pb, Ti, low glue concentrations	High
Vertical	90^0	(100), (110)	High glue concentrations >30mgL^{-1}, solutions containing Pb and glue	High

*Preferred orientations taken relative to ASTM standard for zinc dust

The authors proposed that impurities such as germanium and antimony form some outer sphere complex that stays in solution but significantly catalyzes hydrogen ion reduction. They also suggested that certain crystal orientations will be more favourable for hydrogen evolution and so catalyse it. This is in agreement with the findings of Robinson and O'Keefe (1976). Other impurities such as nickel and cobalt have been found to cause a slight redissolution of the zinc deposit, but this

occurs only after an incubation period that is dependent on the impurity concentration and on the zinc to acid ratio (Mackinnon et al., 1987). As the potential of an electrode resulting from the application of a constant nominal current density depends on the contributions of all the half-cell reactions occurring on the electrode it is possible for the electrode potential to move to a potential more positive than the reversible potential of say zinc, if the rate of a reaction with a more positive reversible potential, e.g. hydrogen, is increased, such as would occur if impurities catalyse it. Localised galvanic effects may also play a role such as when a gas bubble shields the surface from current flow to reduce the cathodic polarization below that required for the plating of zinc. The incubation time is most probably due to the slow accumulation of hydrogen ion reduction catalyst impurities on the surface resulting from their slow mass transfer to the electrode surface at the low concentrations at which they typically occur in electrolytes.

Many impurities interact to either increase or decrease their individual effect on hydrogen evolution during zinc electrowinning. The effect of cobalt and nickel is for instance increased in the presence of antimony (Venkateswaran et al., 1996; Mackinnon et al., 1985) while glue countered the effect of antimony and germanium, but not in the presence of arsenic, titanium, gallium, bismuth and tellurium. Mackinnon et al. (1987) suggested that the change in current efficiency may be a secondary effect caused by the change in preferred orientation of the deposited zinc by the impurities. An impurity like fluoride also indirectly influences the plating of zinc on an aluminium substrate by dissolving the alumina passivation film on the aluminium to allow direct bonding between the metals to significantly increase the bonding of the plated metal to the substrate (Han and O'Keefe, 1992). Fluorides may also indirectly affect the bonding of the zinc to the aluminium cathode possibly through promoting the cementation of impurities and hydrogen evolution catalysts, e.g. copper, directly on the aluminium substrate (Adcock et al., 2002).

2.2.1.4 Acid concentration

Acid in the form of sulphuric acid is typically added to the electrolyte in conventional zinc electrowinning to improve the ionic conductivity of the electrolyte. The benefits of the higher electrolyte conductivity must be balanced with the favouring of the hydrogen ion reduction reaction at higher acid concentrations and thus a higher sensitivity to hydrogen evolution catalysts. Operating at higher acid concentrations is thus only feasible if impurity levels can be kept low consistently, or if the negative effects of gas bubbles on the surface of the electrode can be countered, for instance by limiting their residence time by surfactant additions that increases the hydrophilic nature of the surface.

2.2.1.5 Temperature

The effects of temperature on plating processes are complex as many parameters are influenced by temperature, some of which have already been discussed. Electrochemical reactions are typically more sensitive to temperature than mass transfer processes with the result that mass transfer will, like at lower temperatures, still limit the current density that may be used to obtain good quality deposits at higher temperatures. The nature of the deposit will also be influenced via the effect of temperature on the critical cluster size, via its influence on the surface tension, and on the rate of surface diffusion. Higher rates will favour movement to the most energetically attractive sites, that will typically be those in addition positions at existing electrodeposits, i.e. favouring growth rather than nucleation. Internal stresses in deposits also tend to be lower at higher temperatures possibly due to this effect and or higher rates of solid state diffusion to give some annealing of the structure.

2.3 Development of practically useful parameters and guidelines for the control of electrodeposits

The consideration of the basic processes involved in electrodeposition provides the framework for the understanding of electrocrystallization but is unfortunately not very useful when considering the control of practical electrometallurgical processes. In view of these difficulties Winand (1992, 1994) made major contributions in developing practically useful parameters and guidelines for the control of the morphology of electrodeposited metals, as will be further discussed in the next sections.

Winand (1992) attempted to simplify the prediction of the structure and morphology of electroplated metal using the normalised rate, expressed as the ratio of the current density to the mass transfer limiting current density, and an inhibition intensity, which is inversely related to the exchange current density of the metal plating half-cell to predict the nature of the electrodeposited metal. The inhibition intensity is a characteristic of a certain plating system but can also be modified by the addition of plating inhibitors and modifiers to the electrolyte. Winand proposed a diagram to indicate the conditions for which four main types of deposits could be expected, as first suggested by Fischer (1954), namely the basis orientated reproduction type (BR), field oriented isolated crystals type (FI), field orientated reproduction type (FT), and unoriented dispersion type (UD), as shown in figure 2.6. Other types observed, but not shown on the diagram, are the twinning intermediate type, which overlaps between the FI and FT zones and annotated as (Z), and the nodular (N) and rhythmic lamellar (RL) types which rarely occur. According to Winand the desired

morphology and mechanical properties of an industrial deposit are best achieved as an unoriented dispersion (UD) type deposit, obtained at relatively high inhibition intensities, typically achieved by the addition of organic and inorganic inhibitors, and over a wide range of current densities.

Considering zinc plating specifically, Andersen et al. (1985) classified zinc deposits according to the angle of growth relative to the substrate surface and the effects of impurities and additives on polarization characteristics, as shown in figure 2.7. The grouping of the variables is analogous to the Winand description of BR (basal) at low overpotentials or depolarization by impurities, UD (random) at intermediate potentials with organic inhibition, and FT (vertical) at higher levels of organic inhibition. The uncertainty in the predictability of the deposit type is highlighted by the different UD and FT classifications, compared to that of Winand, and classifying the real deposit in terms of the idealised FT and UD descriptors indicated.

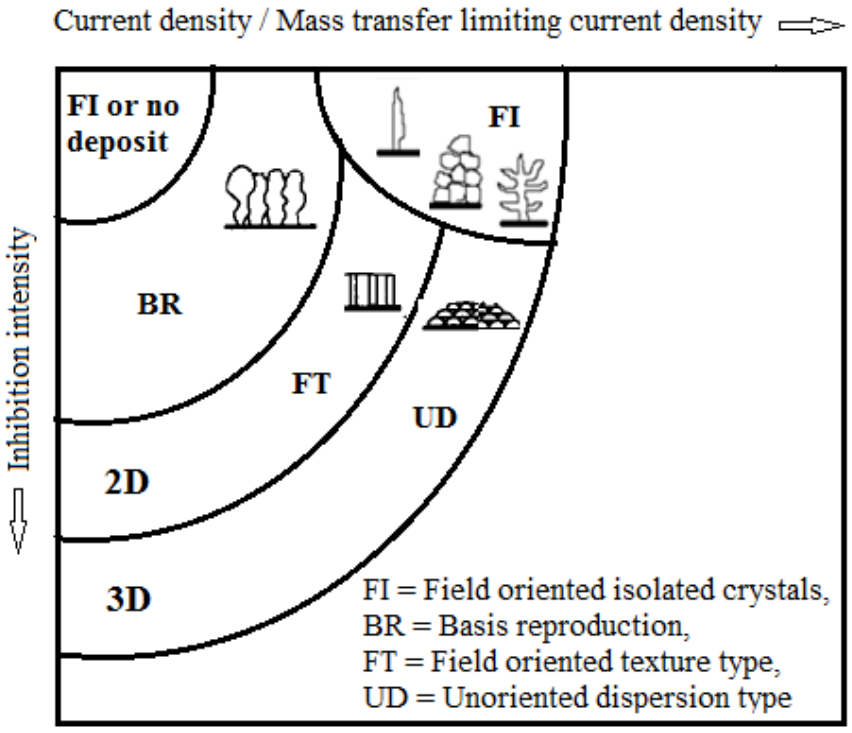

Figure 2.6. Schematic indication of plated metal morphology in terms of the current density ratio and inhibition intensity (After Winand, 1992).

Adcock et al. (2004) further developed the idea and suggested that the classification by Andersen et al. (1985) only considered a single overpotential and electrolyte which may not necessarily produce a unique type of deposit as the nucleation potential may be significantly influenced by different electrolyte parameters and overpotentials. The authors emphasised that the optimal UD structure is obtained by careful control of the nucleation potential (En) and the plating potential (Ep), such that

both nucleation and growth occur during plating. They noted that in Winand's classification the nucleation potential is not explicitly used, but that it is rather inferred from the exchange current density in an additive free electrolyte, thus assuming that it is not affected by additives. Defining the plating potential in terms of a fractional mass transfer limiting current density is also problematic as it is difficult to see how the effect of grain refiners and levelling agents could be sensibly accounted for in such a parameter as they may affect both or only one.

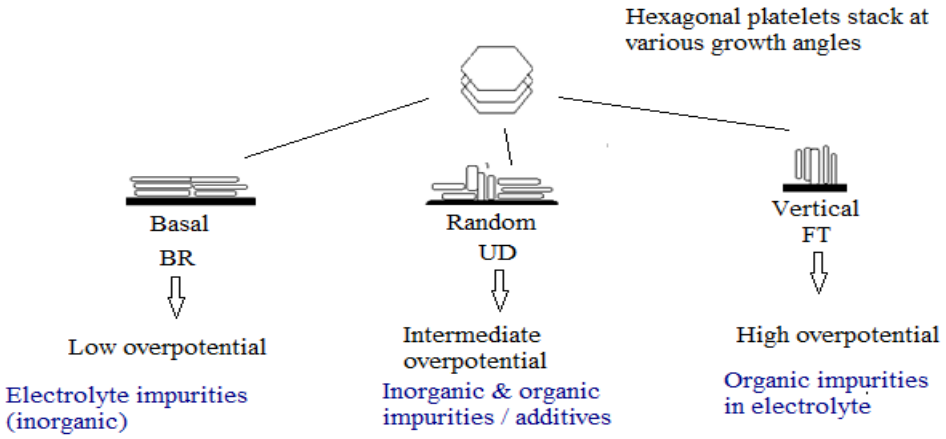

Figure 2.7. Morphological effects of polarization characteristics and various electrolyte compositions in conventional zinc electrowinning (After Andersen et al., 1985).

It is thus clear that although the classifications of Fischer and Winand are valuable for the classification of electroplated deposits their practical application is hampered by the rather lumped nature of the parameters used. Adcock and co-workers suggested the use of a stepped galvanostatic technique, in which the current rather than the potential is controlled, to measure the nucleation potential for zinc plating on an inert foreign substrate, followed by the measurement of the plating potential on the plated zinc.

The nature of a typical galvanodynamic curve is illustrated in figure 2.8, indicating the nucleation potential (En) and the plating potential (Ep). The overpotential for nucleation, ΔE (with ΔE= (En) - (Ep)) is then calculated and plotted against Ep to predict the type of deposit as also indicated in figure 2.9. As expected the desired UD type deposit is obtained at high nucleation and plating potential values for which simultaneous nucleation and growth is predicted. At less cathodic plating potential values nucleation makes a lesser contribution and the growth dominated FT type deposits are formed while at even less cathodic plating potential values the BR and FI types, or no plating, are found.

The choice to control the current rather than the potential in the polarization experiments offers the advantage that the nucleation potential is better defined as the potential typically moves to more positive values after nucleation in galvanostatic experiments due to the lower overpotential required for growth compared to nucleation and a well-defined peak may be measured. When the potential is controlled this is not possible and an increase in current is rather measured. These techniques may also find utility as a complement to chronoamperometry in fundamental electrocrystallization research. For instance, the use of a galvanodynamic scan would provide a good overview of the process for use in deciding suitable limits for chronoamperometric experiments.

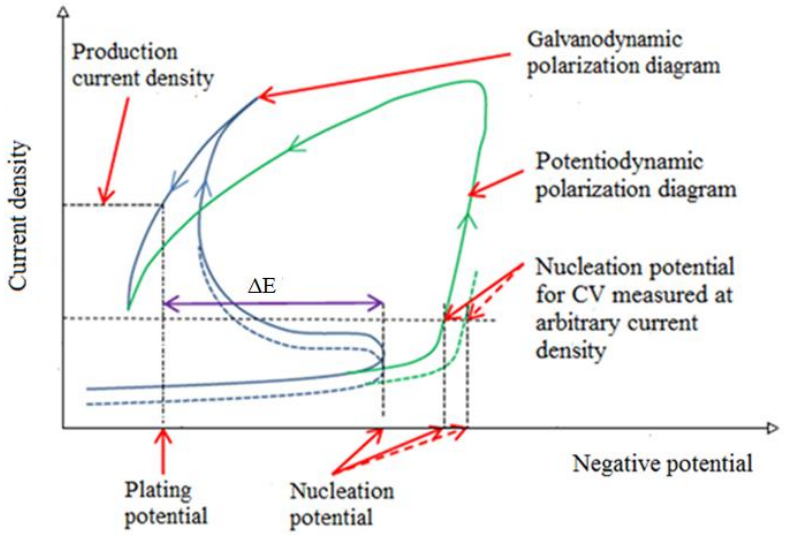

Figure 2.8. Schematic potentiodynamic and galvanodynamic polarization diagrams for zinc plating on an inert substrate from an acid sulphate electrolyte (After Adcock et al., 2002).

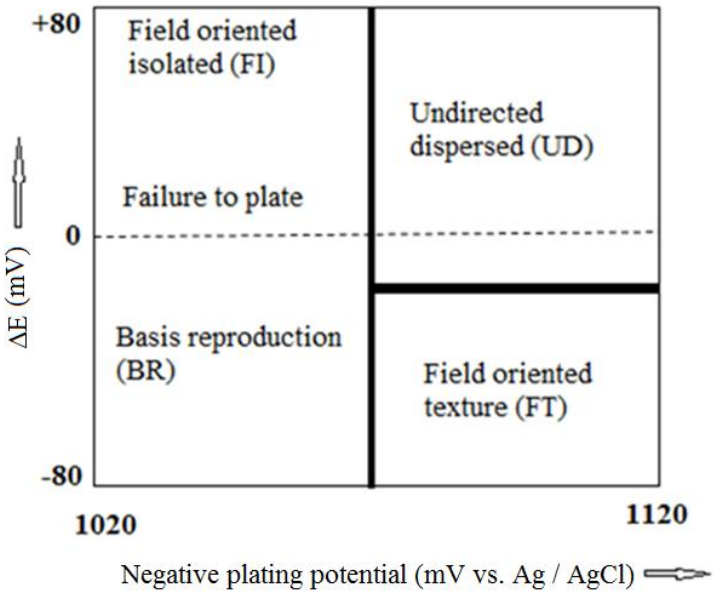

Figure 2.9. Adcock diagram for the prediction of the morphology of plated zinc metal based on the relative values of the nucleation and plating overpotentials for zinc plating on an inert substrate from an acid zinc sulphate electrolyte (After Adcock et al., 2002).

It should also be emphasized that electrochemical nucleation is very sensitive to the potential scan rate and that accurate measurements require that the measured values, which would inevitably include some IR-drop between the electrode and the tip of the Luggin probe of the reference cell, be adjusted, which is easily done retrospectively in the case of galvanodynamic experiments. In the case of potentiodynamic experiments this is not possible as the scan rate itself is affected by the uncompensated IR-drop.

2.4 IR-compensation

In polarization measurements the aim is to measure the potential drop across the diffuse double layer, typically of the order of a nanometre thick, at the interface between the electrode and the electrolyte. As it is not possible to position a reference electrode that close to the surface of the electrode without disturbing the current distribution on the electrode, it is typically positioned much further away from the surface with the result that the measured potential also includes a potential associated with the flow of the current through the electrolyte, i.e. the so called IR-drop, as defined in equation 2.5 and indicated in figure 2.10, with the potential, V, directly proportional to the current, I, passing through the solution such that:

$V = IRs_1$ 2.5

With Rs_1 = Resistance of the solution between the tip of the Luggin tube and the working electrode.

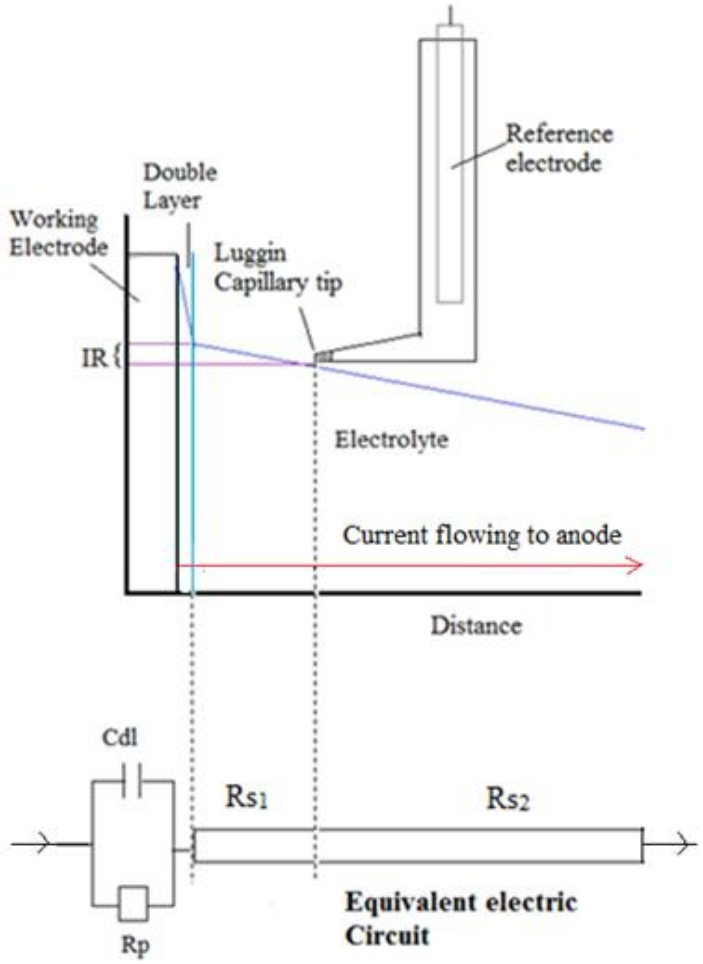

Figure 2.10. Potential distribution and equivalent electric circuit in a three electrode cell. Cdl is the double layer capacitance, Rp is the polarization resistance, Rs_1 is the solution resistance included in the measurements and Rs_2 is the solution resistance between the Luggin capillary tip and the counter electrode.

The calculation of the IR-drop is typically rather complicated as the current distribution close to the electrode is typically not uniform, nor is the composition of the electrolyte, resulting in a non-uniform resistivity of the solution. The situation may be further complicated if gas is evolved at the electrode with the gas bubbles occupying volume but not contributing to the flow of current. It is thus typically more practical to measure rather than calculate the solution resistance between the electrodes for a specific cell set up, with the recognition that it may not be representative of all current densities.

2.4.1 Minimizing the uncompensated resistance

Although including some IR-drop in electrode potential measurements during polarization experiments is inevitable, it is possible to minimize its value. A supporting electrolyte with high ionic conductivity will reduce the resistivity of the solution and therefore also the uncompensated resistance between the electrode and the reference electrode. If the cross sectional area for current conduction of the electrolyte is much larger than that of the electrode the potential drop through the electrolyte would be much reduced although care should be taken not to measure the potential too close to the surface of the electrode as the potential gradient in the electrolyte would be much larger there, and very sensitive to the positioning of the electrode, than further into the electrolyte. A Luggin capillary, i.e. a tube with a fine tip and filled with well conducting electrolyte, can be used to introduce a sensing point close to the electrode without the reference electrode significantly screening the current flow between the electrodes. This is possible because the current flow through the Luggin tube should be very low as a high impedance voltmeter should be used in this circuit, allowing the reference electrode to be positioned some distance away from the electrode, while sensing the potential close to the electrode, and thus decreasing the potential drop measured in the cell electrolyte.

2.4.2 Measuring the uncompensated resistance

The uncompensated resistance can be measured or estimated as discussed in the following sections. The solution resistance can then be used to calculate the electrode potential from the uncompensated measured potential as follows:

$$E = E_{uncompensated} - IRs_1 \qquad 2.6$$

Where: E = Potential that has been corrected for solution resistance, $E_{uncompensated}$ = measured potential, I = Applied current, Rs_1= Solution resistance between the tip of the Luggin tube and the working electrode.

2.4.2.1 Frequency Response Analysis (FRA)

In FRA experiments a cyclical potential perturbation is applied to an interface that is typically controlled at a low overpotential, such that the low field approximation of the Butler-Volmer equation will apply, i.e. that the polarization resistance may be regarded as constant, or at the open

circuit potential to determine the solution resistance. The use of this technique is based on the assumption that the electrical equivalent of the double layer on an electrode can be considered as a resistance in parallel with a capacitance, with the result that the interface will at high frequencies, where the capacitance will have a very low impedance, show negligible resistance to the flow of current and thus allowing the direct measurement of the experimental IR-drop in the electrolyte, as illustrated in figure 2.11.

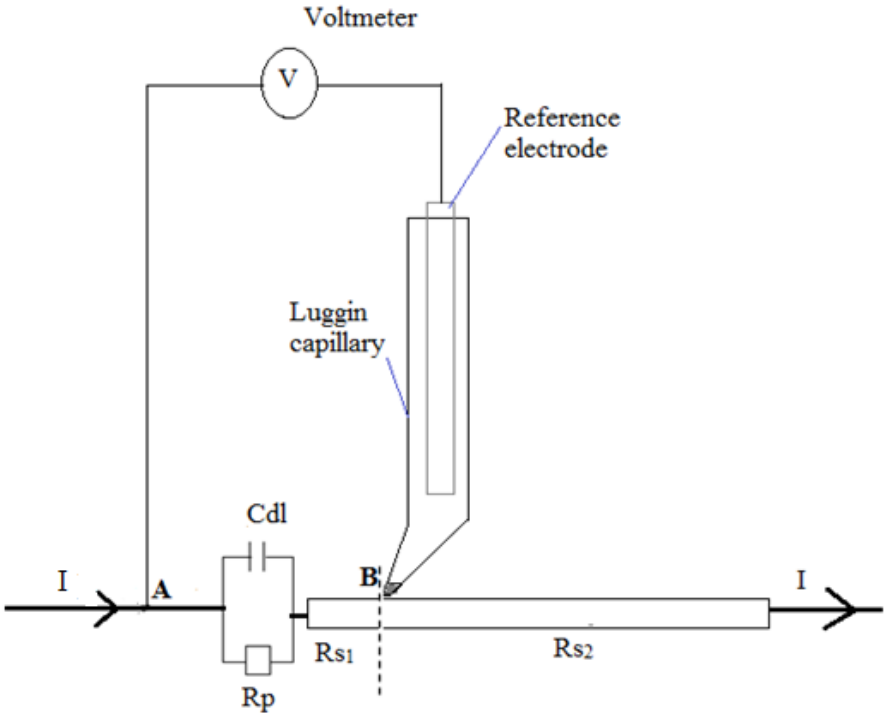

Figure 2.11. The equivalent electrical circuit between the electrode surface and the tip of a Luggin tube with current I passing through them. Where R_p is the charge transfer resistance in parallel to C_{dl}, the double layer capacitance are placed in series with the solution resistancesRs_1, Rs_2.

The frequency dependence of the impedance of the interfacial capacitance is given by:

$$Z_c = \frac{1}{j\omega C_{dl}} \qquad 2.7$$

Where:

$$j = \sqrt{-1} \qquad 2.8$$

$$\omega = 2\pi f \quad (2.9)$$

ω = angular frequency in radians, f = frequency in Hz

The total impedance is given by:

$$Z = R_{s1} + Z' \quad (2.10)$$

The impedance of the parallel circuit, Z' is given by:

$$\frac{1}{Z'} = \frac{1}{R_p} + \frac{1}{1/j\omega C_{dl}} \quad (2.11)$$

This can be simplified to:

$$\frac{1}{Z'} = \frac{1 + R_p (j\omega C_{dl})}{R_p} \quad (2.12)$$

$$Z' = \frac{R_p}{1 + R_p (j\omega C_{dl})} \quad (2.13)$$

Substituting in the equation for total impedance:

$$Z = R_{s1} + \frac{R_p}{1 + R_p (j\omega C_{dl})} \quad (2.14)$$

At low frequency, $\omega \rightarrow 0$, $\Rightarrow Z = R_{s1} + R_p$ (2.15)

At high frequency, $\omega \rightarrow \infty$, $\Rightarrow Z = R_{s1}$ (since $\frac{R_p}{\infty} = 0$) (2.16)

At low frequencies the algebraic sum of $R_p + R_{s1}$is measured since the impedance of the capacitor approaches infinity as the frequency approaches zero. At high frequencies $R_{s1}$is measured because the current short circuits through the double layer capacitor as a result of its lower impedance compared to that of R_p. This can be represented graphically by a Bode plot of the results of the FRA experiment, illustrated in figure 2.12.

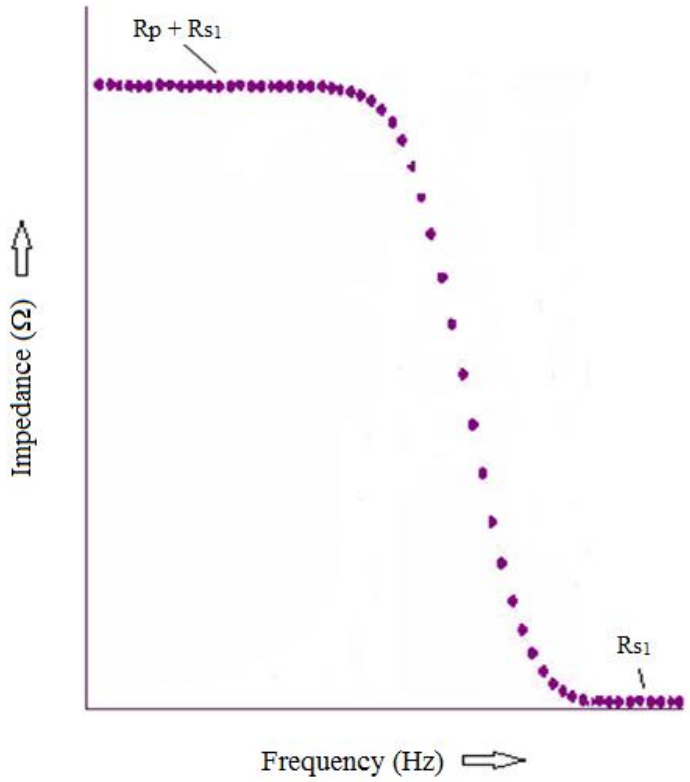

Figure 2.12. Schematic Bode plot showing the measured impedance as a function of frequency. The limiting values of the impedance are equal to ($R_p + R_{s1}$) and R_{s1}, as indicated.

2.4.2.2 Conductivity measurements

The conductivity or resistivity of the electrolyte of the electrolyte can be measured, typically by applying an alternating potential between two electrodes immersed in the electrolyte, such that R_p is short circuited and the only R_{s1} is measured as discussed in the previous section. As the measuring cell is now different from the experimental set up for the polarization measurements the ionic resistance between the electrode and the tip of the Luggin tube must now be estimated considering the resistivity, the current density and the distance between the electrode and the tip of the Luggin tube. For an electrochemical cell, the resistance R_{s1} of the solution is a function of the distance from the tip of the Luggin tube to the cathode surface l(m),the specific conductivity σ, ($\Omega^{-1}m^{-1}$) or (Sm^{-1}) and electrode area, A (m^2) given as;

$$R_{s1}=\frac{l}{\sigma A} \qquad 2.17$$

2.4.2.3 Estimations of specific conductivity from correlations in literature

Barton and Scott, (1992) estimated the specific conductivity σ, ($\Omega^{-1}m^{-1}$) of a zinc sulphate electrolyte as a function of electrolyte composition where, [ ] = Concentration in mol L^{-1}, T= Temperature in K.

$$\sigma=23.92+0.27[H_2SO_4](T-308)+19.6[H_2SO_4]-11.1([Zn^{2+}]+[Mn^{2+}]+[Mg^{2+}]+0.5[NH_4^+] \quad 2.18$$

The results were in excellent agreement with their measured conductivity values. However the effective cross section for current conduction through the polarization cell will typically be bigger than the electrode area with the result that the calculated IR-drop might be slightly larger than that of the polarization cell.

2.5 The role of manganese in zinc electrowinning

Experimental simulation of plant conditions typically involves scaling in electrode type and dimensions and the use of artificial electrolytes to reduce cost and time. However, it is a challenge to decide what species to include in the electrolyte as it may take quite long for an industrial electrowinning plant to reach steady state, if that is ever achieved, as raw materials may change in composition and anodes may take months to build up quasi steady state protective layers. Establishing a representative electrolyte and conditions for experimental studies can be a challenge as species oxidised at the anode, like manganese, may influence the cathodic reactions and need to be reproduced.

Manganese dioxide or potassium permanganate is typically added to the zinc sulphate electrolyte during the leaching and purification processes in order to oxidize and precipitate iron impurities. About 1.5–3 gL^{-1} Mn^{2+} ions are typically required in the electrolyte to minimize lead anode corrosion and to reduce the contamination of the cathodic zinc with lead (Ivanov and Stefanov, 2002). Inspection of the Pourbaix diagram for the Mn-H_2SO_4-H_2O system, shown as figure 2.12, indicates that manganese should be oxidised to species such as $MnO_4^-$and MnO_2 in acidic solutions at the potentials required for the oxidation of water at the anode of a zinc electrowinning cell. These species should also be reduced to $MnSO_4$ at the potentials required for zinc plating and will then affect the current efficiency achieved during zinc electrowinning. The highly oxidised manganese species could also oxidise some impurities, such as arsenic and antimony, to higher oxidation states that could affect their behaviour at zinc plating potentials. Hosny et al. (1989) have shown that low

concentrations of MnO_4^- ions (15–80 mgL^{-1}) in a zinc electrolyte have a beneficial effect on zinc deposition when the electrolyte also contains Sb^{3+} ions, because the oxidation of $Sb^{3+}$to Sb^{5+} ions makes it less harmful to zinc deposition. It thus follows that although manganese will probably not at low concentrations directly influence zinc plating significantly, it would be prudent to include it in simulated electrolytes to more closely simulate conditions found in practice, especially when investigating rather subtle polarization parameters.

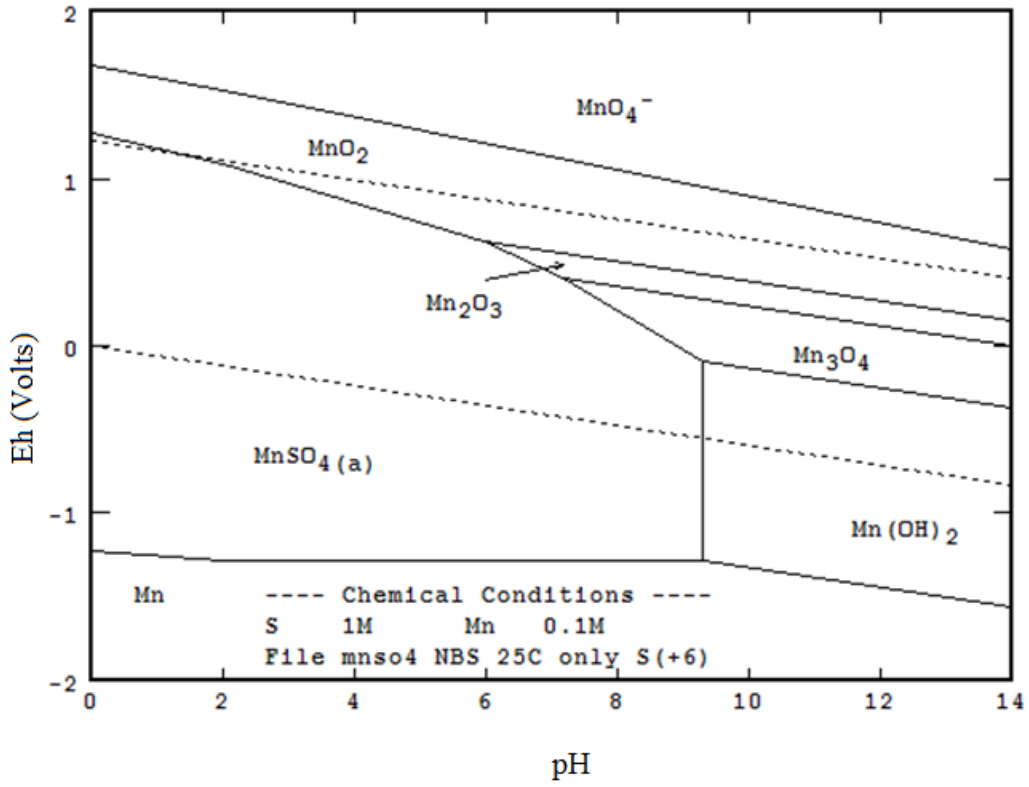

Figure 2.13. Pourbaix diagram for the Mn-H_2SO_4-H_2O system for a soluble manganese species concentration of 0.1M.

2.6 Objectives of this study

The aim of the current work was to further develop and use the galvanodynamic technique for the characterization of zinc sulphate electrolytes to enable prediction of the influence of additives and impurities on the quality of electroplated zinc. The initial work was aimed at the reliable and repeatable measurement of both the nucleation and plating potentials. Once a repeatable two step galvanodynamic technique was achieved, the relationship between the nucleation and plating potential was used as an indicator to optimize the electrolyte and process parameters as well as to

investigate the effect of additives and/or impurities present in the electrolyte on the plating characteristics of the zinc. The most important aim of this work was to determine whether there would exist a definite unique or range of values for both the nucleation and plating potentials for which it would be possible to obtain high quality zinc electrodeposits repeatably. Such a tool would be particularly useful in plant situations to suggest remedies for process upsets and for the evaluation of new additives.

3 EXPERIMENTAL

3.1 Overview

This section describes details of the materials used and experimental methods developed in the course of this investigation including practical details and background theory concerning their use. The first section describes the reagents employed along with relevant information concerning their source and purity. Then the electrode preparation, the electrochemical cell set up, including choice of electrodes and minimization of IR-drop and compensation techniques, environmental control, the instrumentation used for electrochemical polarization experiments and the polarization experiments employed are described. Finally the technique for examination of the structure of the electrodeposits is discussed.

3.2 Reagents

The electrolytes used in electrochemical experiments were prepared using analytical grade reagents and de-ionised water supplied by Merck. The quality of the de-ionised water and the electrolyte was monitored using Induction Coupled Plasma-Optical Emission Spectroscopy (ICP-OES) for the detection of cations. The results indicated no significant traces of critical impurities. The conductivity of the deionised water was measured to be 5.6 μSm^{-1} a characteristic of pure water (Thermo Fisher Scientific, 2014).The level of impurities in the de-ionised water and the electrolyte is shown in table 3.1.

Table 3.1. Level of impurities in the de-ionised water and the standard electrolyte.

	Element concentration in mgL^{-1}						
	Iron	**Copper**	**Nickel**	**Lead**	**Cobalt**	**Chloride**	**Fluoride**
Deionised water	< 0.012	< 0.013	<0.011	<0.052	< 0.012	< 0.011	< 0.020
Standard electrolyte	0.021	<0.010	<0.012	<0.108	< 0.013	< 0.013	< 0.023

An aqueous solution containing 50 gL^{-1} zinc, and 150 gL^{-1} sulphuric acid,H_2SO_4, with 50 mgL^{-1} potassium permanganate, $KMnO_4$, at 38 ^0C was used as the standard electrolyte, representative of industrial electrolytes, to establish the general parameters for the galvanodynamic scans(Rodrigues and Meyer, 1995; Kerby et al.,; 1977; Adcock, 2004). Generally 5 L of stock solution was made up and 0.2 L was used for each electrowinning run such that the electrolyte to working electrode surface area ratio was approximately 200 cm^3:1 cm^2, limiting the change in zinc concentration in the electrolyte to less than 1% during the experiment. Fresh electrolyte was used for each polarization scan. Stock solutions of organic additives were prepared to a concentration of 1 gL^{-1} and were used within a day. The additives were saccharin a brightener and grain refiner in nickel plating (Rashidi and Amaden, 2010), tetrabutylammonium bromide (TBABr) a grain refiner in zinc sulphate electrolytes (Tripathy et al., 1999), pyridine a brightener and leveller for zinc coatings on cast iron (Voss and Hoffmann, 1975) and butyne-1,4-diol a leveller in nickel deposits (Troyon et al., 1995).

The quality of the electrolyte was further evaluated using an anodic stripping test with the prepared working electrode for rapid determination of any trace levels of metal impurities in the electrolytes by observing peaks during the anodic scan as proposed by Bond (1999) and no such peaks were observed.

3.3 Electrode preparation

The working electrode was made of 99.999 % aluminium plate (sourced from Goodfellow Cambridge Limited) with a thickness of 1 mm. The plate was cut into discs with a cross sectional area of 1.13 cm^2.An insulated copper wire was attached at the back of each disc using conductive silver epoxy (Agar Scientific) which was baked at 100 °C for ten minutes to improve the conductivity of the joint. Mounting was thereafter done in Technoviz® 4006 cold curing resin to facilitate polishing of the working surface. This was done by wet polishing to a mirror finish starting with silicon-carbide paper from P600 through P1200 and then P2400 to P4000 grit, and finishing off with 50 nm alkaline colloidal silica slurries on a Mag-Chemal cloth of neoprene material. The polishing material was supplied by Advanced Solutions. After polishing the aluminium electrodes were ultrasonically cleaned in deionised water to remove abrasion debris from the surface and dried in hot air. Prior to reuse, aluminium electrodes were soaked in dilute aqueous sulphuric acid to redissolve the residual zinc before surface preparation using grinding from P1200 grit upwards. After the surface preparation the electrodes were exposed to air for 36 hours to allow for the growth of an oxide film on the aluminium(Adcock, 1999). This effectively

turns the aluminium into an inert substrate from a plating point of view to avoid complications due to interaction between an active aluminium surface and a cementable impurity like copper. The electrodes were weighed before and after the electrochemical experiments.

3.4 Electrochemical cell set up

A conventional three electrode set-up in a perspex cell, fitted with a water mantle to control the temperature, was used for the polarization experiments, as illustrated in figure 3.1. A platinum wire was used as auxiliary electrode and a saturated calomel electrode (SCE) as the reference. The reference electrode was placed in the cell inside a glass tube with a Luggin capillary fitted with a Vycor® tip and filled with 1.2 M potassium sulphate. The tip was positioned 5 mm away from the working electrode surface. The reference electrode was thus at the same temperature as the electrolyte and all potentials were measured relative to the reference electrode at that temperature.

The electrolyte resistance between the tip of the capillary and the working electrode was measured using a frequency response analysis experiment. These experiments involved polarizing the electrode for 5 minutes at the base potential used during normal voltammetry experiments, i.e. at -700 mV (SCE) (Gonzalez-Dominguez, 1994), followed by the application of a small AC signal of, 10 mVrms (root mean square) perturbation in a sine wave format in the frequency range of 100 kHz to 10 mHz (Gabrielli, 1998).The value of the solution resistance was then read off the Bode plot at 100 kHz.

Results from the FRA technique were compared with those from the specific conductivity of the solutions measured using a Tetracon® 325, model Cond 315i conductivity meter, with the resistance between the working electrode and the tip of the Luggin tube estimated based on the distance between the two. The accuracy of conductivity measurements were ≤0.5% of the measured value ± 1 digit and the accuracy of the temperature measurements were ≤0.1% °C ± 1 digit. They were also compared with those from correlations in literature. The measured plating potential was then corrected by subtracting the calculated IR-value to obtain the real value.

Temperature control was achieved throughout the experiment with an external circulating water bath which had an internal heating coil in combination with a thermocouple with an accuracy of ±1 °C.

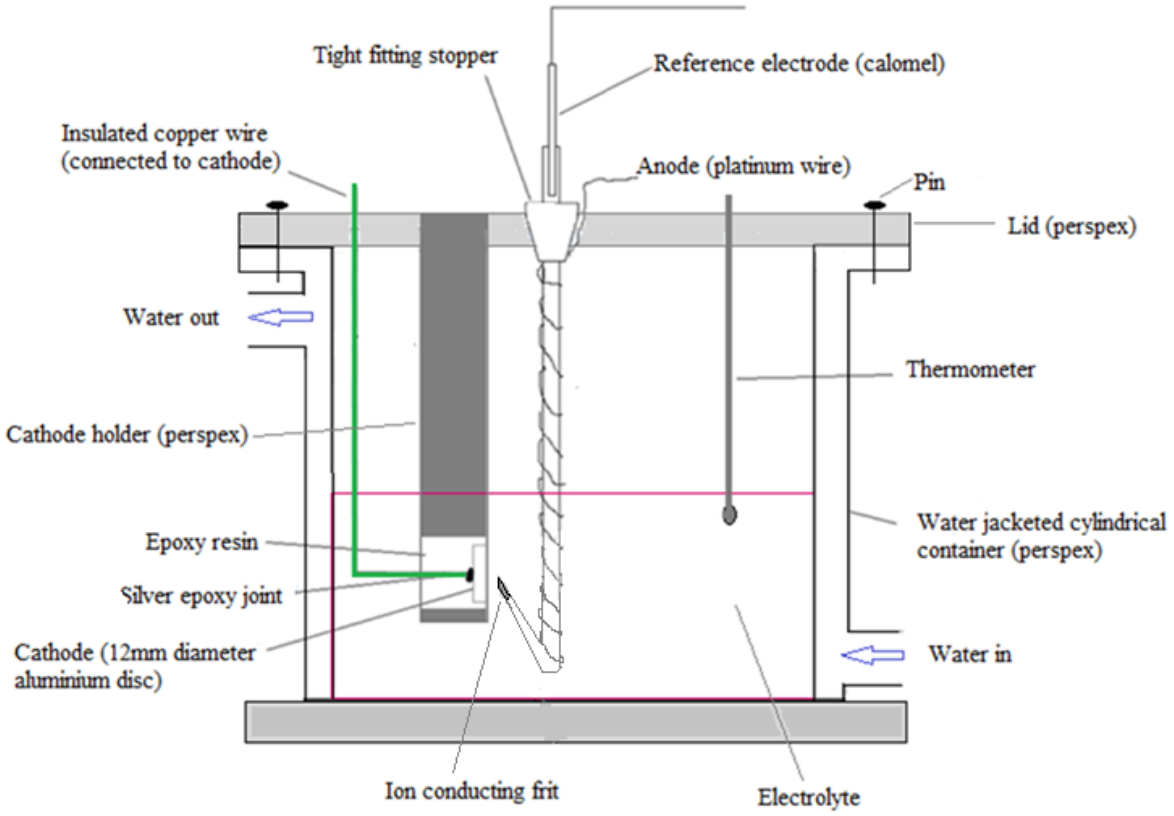

Figure 3.1. Schematic representation of the electrochemical cell set-up.

3.5 Experimental method for measuring polarization.

The polarization experiments were done using a Solartron Schlumberger 1286 interface connected to a computer to control the interface and record the data. The interface was used in the galvanostatic mode. The working electrode was introduced into the cell containing the electrolyte and left for 20 seconds at zero current to allow for stabilization. The galvanodynamic parameters selected for this study are indicated in figure 4.1. To define the nucleation potential accurately a slow initial scan rate of 0.0125 $mAs^{-1}$was used, but the plating potential was not that sensitive to the scan rate and the use of a faster rate of 0.585 $mAs^{-1}$for the second stage simplified the experiment. These scan rates were within the range of values recommended by Adcock(1999) Following the galvanodynamic scans to determine the nucleation and plating potentials, the program instantly shifted to the galvanostatic deposition of the zinc, which was done for 80 minutes (Adcock et al.,2004) at a typical industrial plating current density of 600 Am^{-2}(Van Dyk, 2006).

The current efficiency for zinc plating was calculated by comparing the mass deposited to the theoretical mass that should have been deposited according to Faraday's law. Raw data on the mass

measurements is given in appendix F. A typical calculation of theoretical mass is shown in appendix E.

3.6 Examination of electrodeposits

After completion of the plating cycle the cathode was cleaned in deionised water and left to dry.. It was then weighed and the difference between the cathode mass before and after deposition was taken as the mass of the plated metal.

The plated metal was then stripped manually using a sharp thin blade to lift the edges, cross-sectioned, mounted in epoxy resin and polished down to a 1 μm diamond finish. The microstructures were inspected optically after etching with 0.1 M sodium hydroxide for 2 seconds, swabbing with an aqueous solution containing 200 gL^{-1} CrO_3 and 15 gL^{-1} Na_2SO_4 for 2 seconds (Adcock, 1999), flushing with anhydrous alcohol and deionised water and finally drying in hot blowing air.

4 RESULTS AND DISCUSSION

4.1 Potential measurement error

The resistance between the tip of the Luggin probe and the aluminium cathode was measured for the standard electrolyte of 50 gL^{-1} zinc solution with 150 gL^{-1} sulphuric acid and 50 gL^{-1} potassium permanganate at 38^0C using frequency response analysis and was found to be 1.070 Ω ± 0.003 Ω. The specific conductivity, σ, was measured to be, 43.5 $\Omega^{-1}m^{-1}$ ± 0.1 $\Omega^{-1}m^{-1}$. The distance of the Luggin tube tip from the cathode was 0.005 m, and the area of the electrode surface was 1.13 x 10^{-4} m^2. Therefore the solution resistance was calculated using equation 2.16 as:

$$R_s = \frac{l}{\sigma A} = \frac{0.005m}{43.5\Omega^{-1}m^{-1} \times 1.13 \times 10^{-4}m^2} = 1.02\ \Omega$$

The relatively minor difference indicate that the geometry of the polarization cell did not significantly affect the voltage drop and that calculated values for the resistance between the electrode and the tip of the Luggin probe may be used for doing the IR-drop.

The resistance was also calculated using the correlation of Barton and Scott (1992) given as equation 2.18:

$$\sigma = 23.92 + 0.27[H_2SO_4]\,(T - 308) + 19.6[H_2SO_4] - 11.1([Zn^{2+}] + [Mn^{2+}] + [Mg^{2+}] + 0.5[NH_4^{+}]). \qquad 2.18$$

Substituting for the temperature of 38 ^{0}C and concentrations of the species in the electrolyte in the equation gives:

$$\sigma = 23.92 + 0.27[1.5]\,(311 - 308) + 19.6[1.5] - 11.1([1] + [0.0004] + [0] + 0.5[0])$$

$$\sigma = 43.4\ \Omega^{-1}m^{-1}$$

The solution resistance was then calculated again using equation 2.16 as:

$$R_s = \frac{l}{\sigma A} = \frac{0.005m}{43.4\Omega^{-1}m^{-1} \times 1.13 \times 10^{-4}m^2} = 1.02\ \Omega$$

The magnitude of the measurement error is a function of the resistance of the solution and for strong electrolytes is typically small enough to be neglected, unless very accurate measurements are required such as is the case in the present study where potential differences of the order of one millivolt is significant. For example, with a solution resistance of about one ohm between the electrode and the sensing point about 5 mm from the electrode, measured using frequency response analysis for this specific set up, a current of 60 mA (equivalent to a current density of 600 Am^{-2} on a $1x10^{-4}$ m^2 electrode) will cause a measurement error of 60 mV, which cannot be ignored for most measurements and certainly not in the present context.

The use of frequency response analysis to determine the solution resistance between the working electrode and the point of the Luggin tube was used to avoid the complications associated with estimating the resistance using the solution resistance for a cell set-up with a working electrode of smaller surface area than the cross section of the electrolyte with a resultant non-uniform current distribution through the electrolyte.

The magnitude of the potential error adjustments in the present work ranged from 0.5 mV for the nucleation potentials, where the small currents flowing resulted in minimal error, to the mentioned 60 mV at the plating current density of 600 Am^{-2}. The actual corrections applied are summarized in appendix B.

The values for the frequency response analysis experiments for the different electrolytes are given in table 4.1, shown later with the polarization results. More detailed results showing their repeatability is given in Appendices C and D. As expected the electrolyte resistance decreased with increasing acid concentration and increased with increasing zinc concentration, but was relatively insensitive to the presence of minor species in the electrolyte.

4.2 Polarization characteristics

A typical galvanodynamic polarization diagram obtained for zinc plating from the aqueous acid sulphate electrolyte, after IR-correction of the potential, is shown in figure 4.1. The nucleation potential peak is clearly visible as the most negative potential reached during the initial stage of the scan. In this particular case the nucleation potential was about 0.1 V more negative than the reversible potential for plating or dissolution of the zinc. The plating potential again moved to more negative potentials with increasing current densities and then levelled off to a broad peak. Also note that in this case the plating potential, read off at an industrially relevant current density of 600 Am^{-2},

was less negative than the nucleation potential, indicating that growth of the deposit rather than the nucleation of new grains should be favoured according to the proposed theoretical considerations in the literature (Adcock, 1999).The plating potential was read off during the reverse scan because it was more reproducible compared to the forward scan. The reverse scan occurs on a zinc covered electrode which could be the reason why the gradient which represents the resistance is constant compared to that on the forward scan where surface area is changing and hence resistance is changing with deposition. Good repeatability was obtained for both potentials, e.g. typically within 3 mV for repeat runs, when strictly adhering to the cathode preparation and experimental procedures. The results for the nucleation and plating potential measurements are shown in appendices A and B.

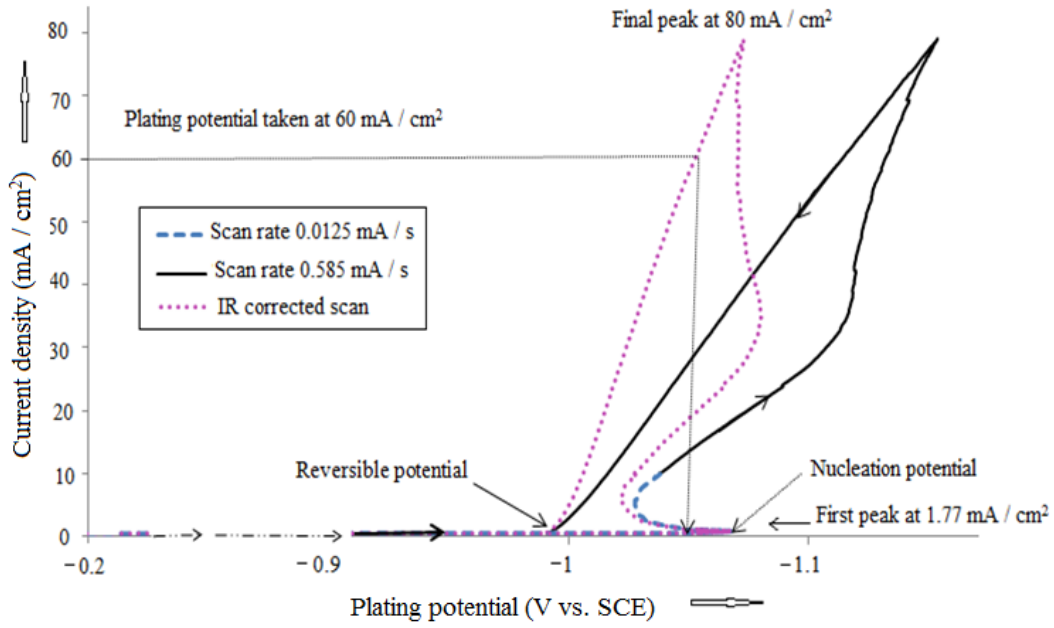

Figure 4.1. Galvanodynamic polarization diagram for zinc plating on an aluminium cathode from an aqueous zinc sulphate solution containing 50 gL^{-1} zinc, 150 gL^{-1} sulphuric acid, and 50 mgL^{-1} potassium permanganate at 38 ^{0}C. The dotted line shows the scan after correcting for the IR-drop measurement error.

4.3 Microstructural characterization of deposits

Typical microstructures observed on cross sections of the zinc deposits obtained at different electrolyte compositions are shown in figure 4.2 (a) to (d).

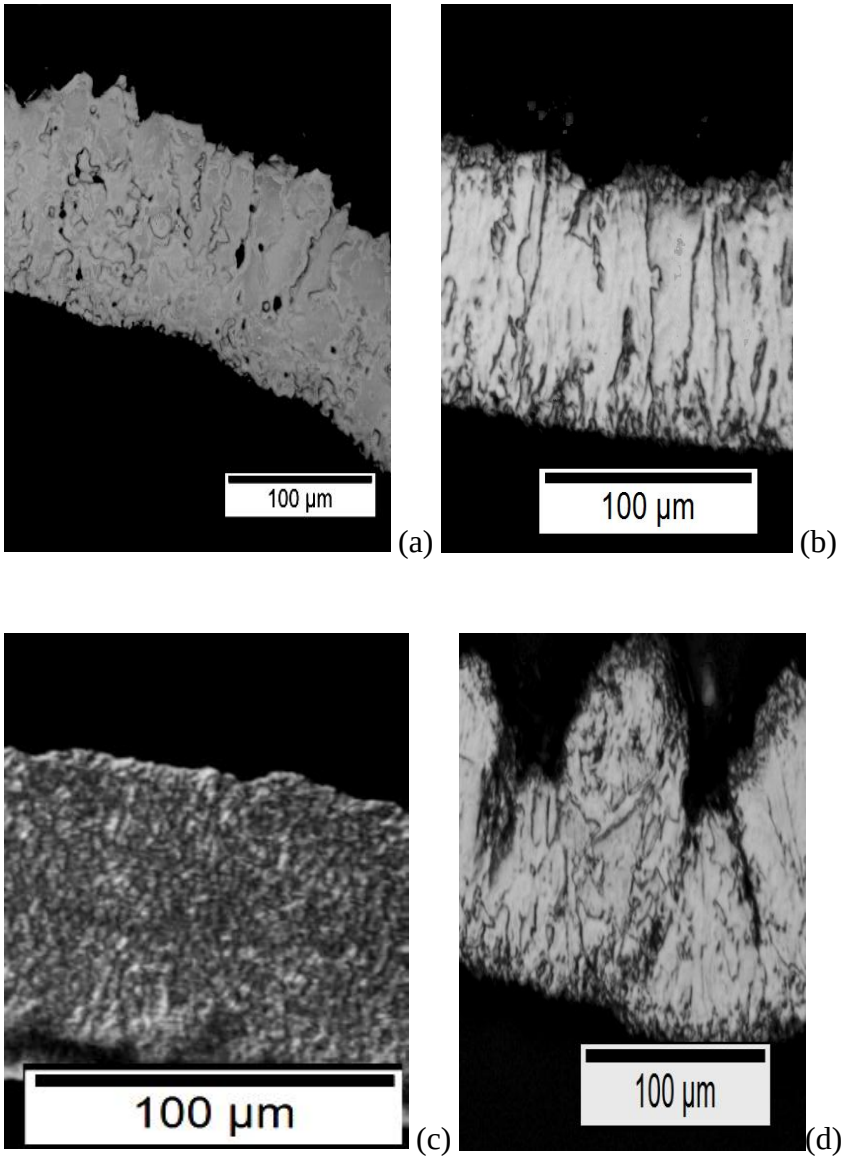

(a) (b) (c) (d)

Figure 4.2. Micrographs for zinc plating on aluminium from an aqueous acid zinc sulphate solutions containing (a) 50 gL^{-1} zinc, 200 gL^{-1} sulphuric acid, and 50 mgL^{-1} potassium permanganate at 38^{0}C (b) 30 gL^{-1} zinc, 150 gL^{-1} sulphuric acid, and 50 mgL^{-1} potassium permanganate at 38^{0}C (c) 50 gL^{-1} zinc, 150 gL^{-1} sulphuric acid, 50 mgL^{-1} potassium permanganate and 10 mg L^{-1} TBABr at 38^{0}C (d) 50 gL^{-1} zinc, 200 gL^{-1} sulphuric acid, and 50 mgL^{-1} potassium permanganate at 60^{0}C. The micrographs were taken near the middle of the deposits.

The structure shown in figure 4.2 (a) is an example of the basis orientated reproduction (BR) type, which according to Winand (1992) would typically be obtained at relatively low normalised current densities and low degrees of inhibition and low overpotentials according to Andersen et al. (1985). These deposits were rough and columnar with very large grains whose width grew even broader with deposition time. The boundaries between the crystallites were somewhat separated and allowed for some electrolyte entrapment. These deposits were very ductile and easy to strip. The structure shown in figure 4.2 (b) resembles the (FT) type which consisted of tight columnar grains smaller in width than the BR type, was relatively level and formed at higher plating potentials and also had good ductility and strippability. The deposit shown in figure 4.2(c) exemplifies the unoriented dispersion type (UD) consisting of small equiaxed grains which would typically be expected if significant nucleation of new grains occurs during the plating process. These deposits were very compact, relatively well levelled and easily strippable. Structures represented in figure 4.2 (d) were degraded BR structures that were nodular, stressed and non-coherent. These could well be classified as FI structures expected to be formed at both low and high normalised current densities with low inhibition intensity according to the Winand classification. In summary it can be stated that the UD type deposits would be optimal in terms of mechanical properties and smoothness, while the FT and BR types can be expected to have lesser but still acceptable mechanical properties, but probably of lower chemical quality due to possible entrainment of the electrolyte inside and on the surface of the plated metal, while the FI type deposits would be undesirable in terms of mechanical as well as chemical quality considerations.

4.4 Correlating the polarization characteristics with the metallographic structure

The suggestion by Adcock et al. (2004) that the type of electroplated deposit can be predicted using galvanostatic polarization measurements was further evaluated for electrolytes of varying zinc and acid concentrations and at various electrolyte temperatures, as well as for electrolytes containing additives such as saccharin, tetrabutylammonium bromide, pyridine and butyne-1, 4, diol.

The grouping of the microstructural types in terms of the polarization characteristics, i.e. En, Ep, and ΔE= En- Ep, as proposed by Adcock et al. (2004) into five regions with similar polarization characteristics, current efficiencies, and microstructure are indicated in table 4.1 and figure 4.3

The present work indicates that the type of deposit obtained for zinc plating from a sulphate electrolyte can be delineated using the potential difference (ΔE) between the nucleation potential (En) and the plating potential (Ep), and plating potential (Ep) as parameters, as illustrated in figure

4.3. It is also clear that the difference between (En) and (Ep), i.e. ΔE, plays a determining role for the type, quality and characteristics of the deposit formed.

It is again necessary to mention that although significant variations occurred within the broad plated metal morphologies and characteristics, only the mixed FT and BR and FI types would be unacceptable due to the low current efficiencies recorded and the overall quality and character of the deposits. The most desirable quality deposits were found in the UD and FT regions as shown in figure 4.3. An uncertainty in the predictability of the deposit type between UD and FT classifications was also found as in the literature, i.e. classifications of Andersen et al. (1985) compared to those of Winand, (1992). Distinguishing between FT and UD type deposits will require further SEM and XRD and other physical property measurements such as hardness, grain size and ductility. This will complicate the analysis and probably not be worthwhile as both the UD and some FT type deposits have good adhesion, no dendrites or other protrusions, acceptable grain size, no pinholes, as well as high current efficiencies. The UD and FT regions indicated in figure 4.3 are therefore considered the most likely regions in which the most desirable quality deposits will be obtained.

Table 4.1. Electrolyte compositions, measured polarization parameters (En, Ep, ΔE), current efficiency (CE), solution resistance (Rs), and the morphology of the electroplated zinc

[Zn]	$[H_2SO_4]$	Temperature	Additive	En	Ep	ΔE	CE	R_s	Region
(gL^{-1})		(°C)	(mgL^{-1})	(mV vs. SCE)		(mV)	(%)	(Ω)	
10	150	38	None	-1104	-1114	10	63	0.81	FT and BR
30	150	38	None	-1090	-1071	-19	98	0.92	FT and UD
40	150	38	None	-1078	-1064	-14	99	0.99	FT and UD
60	150	38	None	-1089	-1045	-44	99	1.06	FT and UD
80	150	38	None	-1075	-1032	-43	99	1.08	FT and UD
90	150	38	None	-1035	-1017	-18	77	1.23	BR
100	150	38	None	-1050	-1055	5	76	1.3	FT and BR
120	150	38	None	-1033	-1036	3	74	1.44	FT and UD
50	0	38	None	-1055	-991	-64	61	9.06	BR
50	10	38	None	-1092	-953	-139	73	6.23	BR
50	50	38	None	-1080	-1067	-13	77	2.59	FT
50	100	38	None	-1075	-1034	-41	82	1.4	BR
50	200	38	None	-1091	-1020	-71	84	0.87	BR
50	250	38	None	-1083	-1017	-66	97	0.76	BR
50	150	20	None	-1103	-1099	-4	81	1.18	FT and UD
50	150	30	None	-1092	-1095	3	83	1.09	FT and BR
50	150	40	None	-1057	-1015	-42	98	1.07	BR
50	150	50	None	-1006	-1012	6	62	0.9	FI
50	150	60	None	-1004	-1004	0	45	0.8	FI
50	150	70	None	-996	-1005	9	30	0.7	FI

Table 4.1. Continued

[Zn]	$[H_2SO_4]$	Temperature	Additive	En	Ep	ΔE	CE	R_s	Region
(gL^{-1})		(°C)	(mgL^{-1})	(mV vs. SCE)		(mV)	(%)	(Ω)	
			TBABr						
50	150	38	2	-1048	-1030	-18	87	0.95	FT and UD
50	150	38	5	-1045	-1042	-3	91	0.95	FT and UD
50	150	38	10	-1093	-1082	-11	86	0.95	FT and UD
50	150	38	40	-1081	-1078	-3	86	0.96	FT and UD
50	150	38	100	-1100	-1083	-17	80	0.97	FT and UD
			Saccharin						
50	150	38	2.5	-1050	-1040	-10	75	0.95	UD and FT
50	150	38	5	-1129	-1043	-86	68	0.95	FT
50	150	38	15	-1117	-1081	-36	87	0.95	FT and BR
50	150	38	25	-1063	-1077	14	72	0.95	FT and BR
50	150	38	40	-1041	-1076	35	60	0.95	FT and BR
50	150	38	60	-1122	-1138	16	55	0.95	FT and BR
50	150	38	80	-1141	-1160	19	40	0.96	FT and BR
50	150	38	100	-1139	-1120	-19	31	0.98	FT

Table 4.1. Continued

[Zn]	$[H_2SO_4]$	Temperature	Additive	En	Ep	ΔE	CE	R_s	Region
(gL^{-1})		(°C)	(mgL^{-1})	(mV vs. SCE)		(mV)	(%)	(Ω)	
			Pyridine						
50	150	38	1	-1174	-1121	-53	70	0.98	FT
50	150	38	5	-1155	-1120	-35	66	0.97	FT
50	150	38	10	-1125	-1104	-21	70	0.97	UD and FT
50	150	38	20	-1134	-1101	-33	66	0.97	UD and FT
50	150	38	30	-1129	-1094	-35	67	0.96	UD and FT
50	150	38	40	-1122	-1085	-37	68	0.97	UD and FT
50	150	38	55	-1125	-1090	-35	67	0.97	UD and FT
50	150	38	70	-1141	-1101	-40	69	0.97	UD and FT
50	150	38	85	-1135	-1105	-30	63	0.97	FT
50	150	38	100	-1129	-1109	-20	60	0.98	FT
			Pyridine; Saccharin						
50	150	38	10;100	-1187	-1156	-31	27	1.01	FT
50	150	38	40;40	-1151	-1185	-34	36	0.99	UD and FT

Table 4.1. Continued

[Zn]	[H_2SO_4]	Temperature (°C)	Additive (mgL^{-1})	En (mV vs. SCE)	Ep	ΔE (mV)	CE (%)	R_s (Ω)	Region
			Butyne-1,4, diol						
	150	38	1	-1139	-1130	-9	76	0.98	FT
	150	38	3.5	-1135	-1125	-10	75	0.98	FT
50	150	38	5	-1132	-1119	-13	77	0.99	UD and FT
50	150	38	10	-1136	-1107	-29	76	0.99	UD and FT
50	150	38	15	-1134	-1086	-48	75	0.97	FT
50	150	38	20	-1120	-1070	-50	76	0.98	FT
50	150	38	25	-1110	-1056	-54	74	0.98	FT
50	150	38	30	-1135	-1078	-57	76	0.98	FT
50	150	38	40	-1141	-1100	-41	78	0.97	UD and FT
50	150	38	50	-1129	-1102	-27	77	0.98	UD and FT
50	150	38	60	-1120	-1105	-15	76	0.99	UD and FT
			$KMnO_4$						
50	150	38	25	-1138	-1203	65	78	0.99	FT and BR
50	150	38	37.5	-1063	-1027	-36	79	1	UD and FT
50	150	38	50	-1057	-1015	-42	81	1	UD and FT
50	150	38	75	-1044	-1077	33	83	1.02	FT and BR
50	150	38	100	-1064	-1071	7	77	1.04	UD and FT

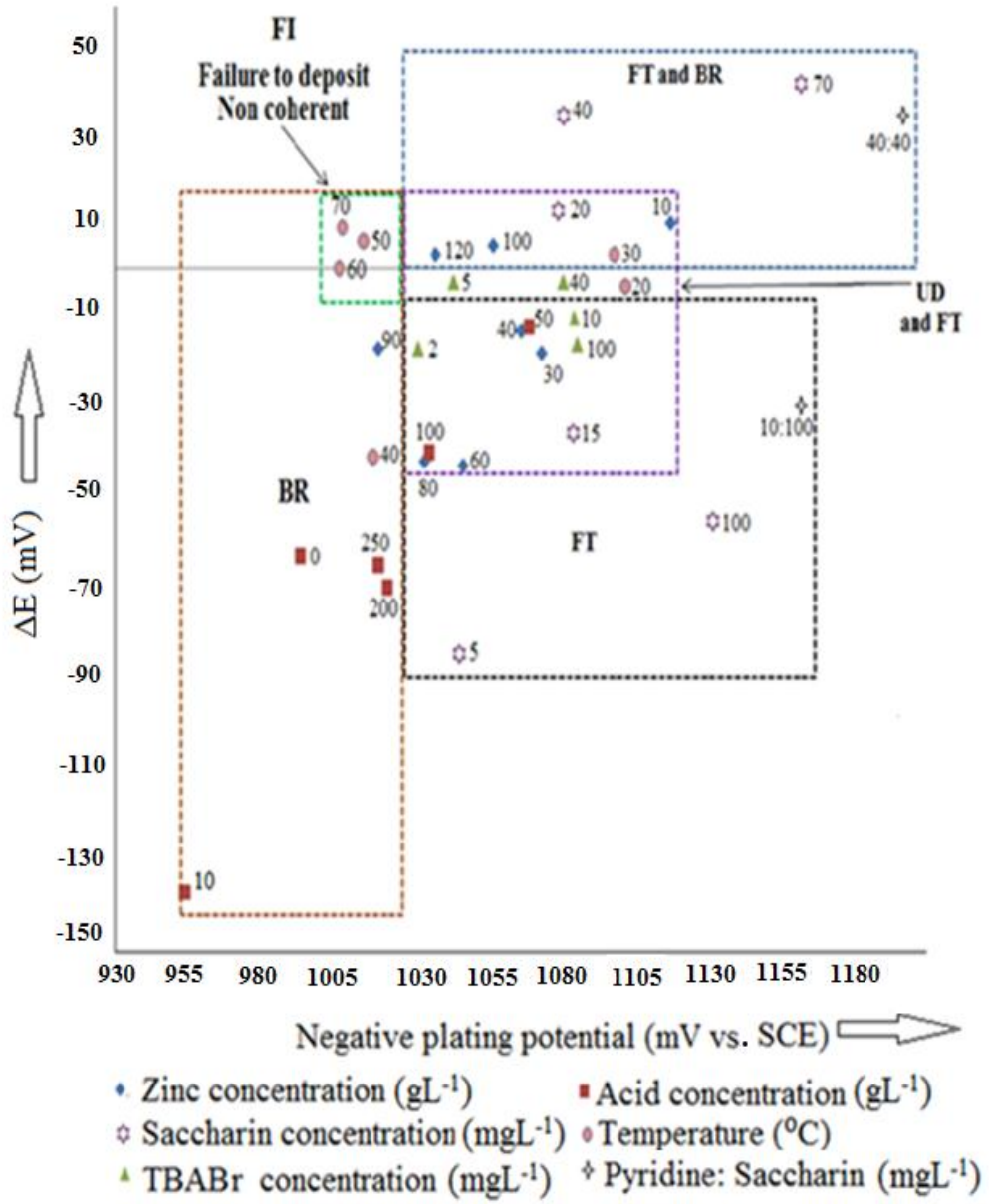

Figure 4.3. Correlation between the microstructure of electroplated zinc metal and the measured polarization characteristics. Numbers refer to the concentration of the species varied in the electrolytes listed in table 4.1.

The results from the current study clearly show that the En and Ep values for each specific condition as well as the relationship between En and Ep, i.e. ΔE, can be used as a measure of the relationship between nucleation and growth processes. The conditions for the different types are in broad agreement with those found by Adcock et al. (2004) but the region for the typically desired unoriented dispersion (UD) type of deposit is more limited and not obtained at more positive ΔE values, but is found at negative ΔE where field oriented texture (FT) and basis reproduction (BR) types are again found. This agrees with findings of Adcock (2004). This indicates that the premise that three dimensional nucleation, with a resultant finer grain size and unoriented growth, will be favoured at a positive overpotential for nucleation compared to plating, i.e. for positive values of ΔE, may not be invariably so. This is further illustrated by the UD deposits found at negative ΔE values where growth should be favoured over nucleation, as is indeed found at more negative values of ΔE. This could presumably be because the initial nucleation potential will be high due to zinc nucleation on aluminium as the initial monolayer is formed. As zinc is plated over the aluminium, further nucleation will be for zinc on zinc with less negative plating potentials. However, in the presence of grain refiners frequent nucleation is always promoted relative to growth such that even for zinc plating on zinc nucleation potentials may shift slightly to less negative values but are controlled and maintained close to those of the initial nucleation such that there will not be a significant difference between the nucleation and plating potentials.

Based on the classification made in figure 4.3 a detailed discussion on the effect of the various parameters investigated on polarization parameters and morphology will be done in the next sections.

4.4.1 Zinc concentration

It can be seen from figure 4.4 that both the nucleation and plating potentials are influenced by the concentration of the zinc ions in solution in different ways and therefore it is important to consider both these parameters when making any prediction of the morphology as indicated by Adcock et al., (2002). It is clear that both the nucleation and plating potentials become more positive with increasing zinc concentration. A general decrease in polarization with increasing zinc concentration is in agreement with the findings of Lee and Jorne (1992). This could be attributed to the reduced activity of hydrogen as the concentration of zinc increases. This is also evidenced by an increase current efficiency in agreement with experimental observations of Wark (1979) and Scott et al. (1988). The plating potential reaches a pronounced minimum around 90 gL^{-1} with random behaviour at higher concentrations. The influence of the zinc concentration on ΔE is shown in figure 4.5. For zinc concentrations less than about 25 gL^{-1} ΔE is positive, i.e. the nucleation potentials are smaller than the plating potentials and small grains are predicted but not found. From 25 to 80 gL^{-1} zinc, which is typical of present industrial practice, ΔE is negative and the grains were slightly coarser FT type as would be predicted. For zinc concentrations above about 100 gL^{-1} ΔE becomes slightly positive again and sought after FT and UD type deposits are obtained. It can be concluded from these results that the quality of the deposited zinc is relatively insensitive to the zinc concentration at an acid concentration of 150 gL^{-1}, which is typically used in practice, with generally good and acceptable FT type deposits with good ductility and strippability. The grain size of the zinc seems to remain constant over a wide range of concentrations regardless of the change in potentials and ΔE.

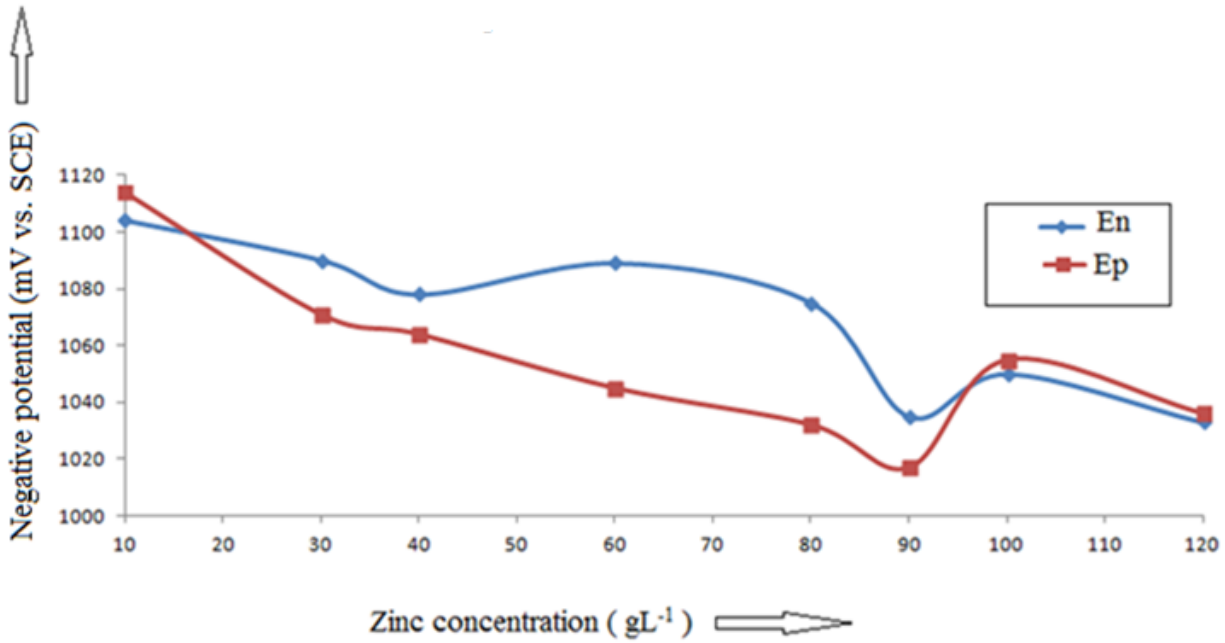

Figure 4.4. Influence of the zinc concentration on the nucleation and plating potentials with zinc concentrations for a solution containing 150 gL^{-1} sulphuric acid at 38 ^0C.

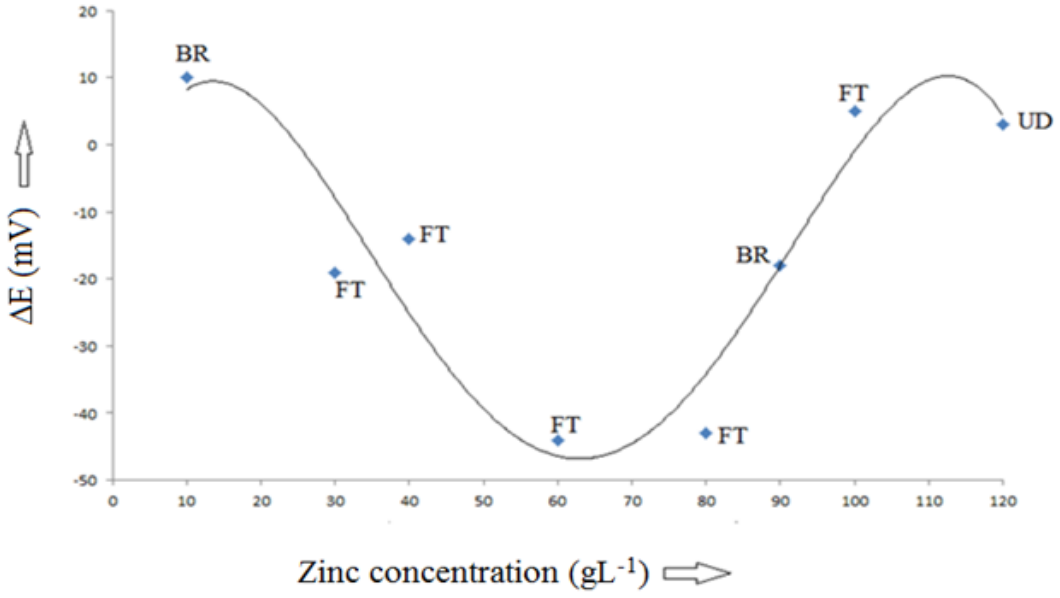

Figure 4.5. Influence of zinc concentration on the difference between nucleation and plating potentials for a solution containing 150 gL^{-1} H_2SO_4 at 38 °C.

4.4.2 Acid concentration

The influence of acid concentration on the nucleation and plating potentials is shown in figure 4.6 indicating that the nucleation potential is relatively insensitive to acid concentration but that the plating potential becomes more negative at low concentrations and then becomes more positive at concentrations higher than 50 gL^{-1} sulphuric acid. The increase to more negative potentials at higher concentrations may be due to the inhibiting effect of acid on zinc deposition in agreement with observations of Epelboin et al. (1975). ΔE as a function of acid concentration is shown in figure 4.7 and indicates that the desired FT plating structures are obtained at small ΔE values and that at the larger ΔE values obtained at low and high acid concentrations zinc deposits with the less desirable BR plated structure are obtained.

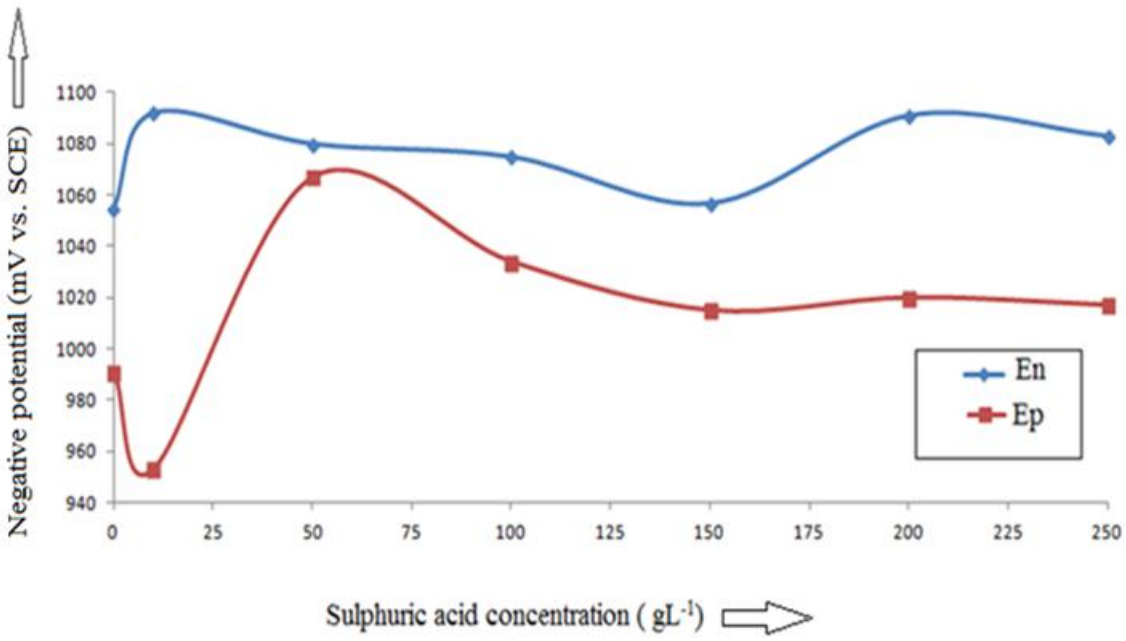

Figure 4.6. Influence of acid concentration on the nucleation and plating potentials for a solution containing 50 gL^{-1} zinc at 38 ^{0}C.

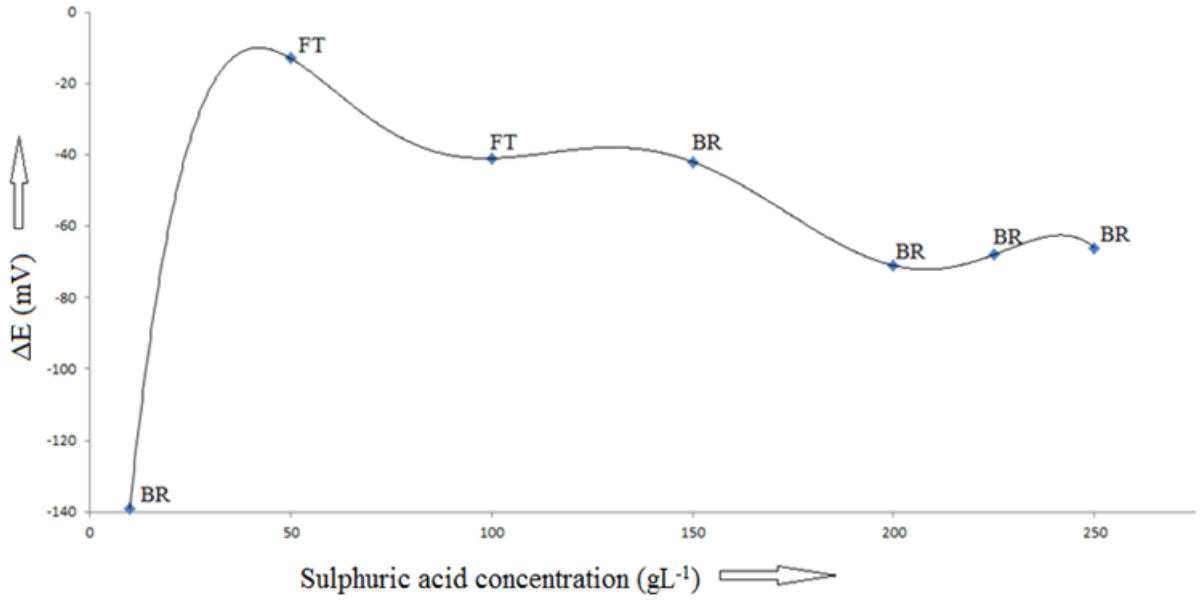

Figure 4.7. ΔE and plated zinc structure as a function of sulphuric acid concentration for a solution containing 50 gL^{-1} zinc at 38 °C.

4.4.3 Temperature

The influence of temperature on the plating characteristics is not very significant at both low and high temperatures with a transition between 30 and 50 °C as indicated in figures 4.8 and 4.9. Scott et al. (1988) also observed a drop in cathodic potentials in an almost similar range of temperatures. The move to more positive nucleation and plating potentials at higher temperatures is probably due to an increase in the rate of hydrogen ion reduction which would tend to move the potential at which a significant current flow, but not necessarily due to zinc plating, to more positive potentials. Zinc dissolution or hydrogen ion reduction should also significantly decrease the current efficiency at higher temperatures as was indeed found to be the case. It also follows that the approach to characterise zinc plating by polarization characteristics is probably not valid for conditions where significant rates of hydrogen ion reduction occur. The results show that deposits degrade with increasing temperatures. Scott et al. (1988) also reported a deterioration in the quality of zinc deposits with increasing temperature above 45°C.

The results therefore indicate that the quality of the plated zinc from additive free electrolytes may be improved by operating at lower temperatures where UD and FT structures were obtained at higher current efficiencies.

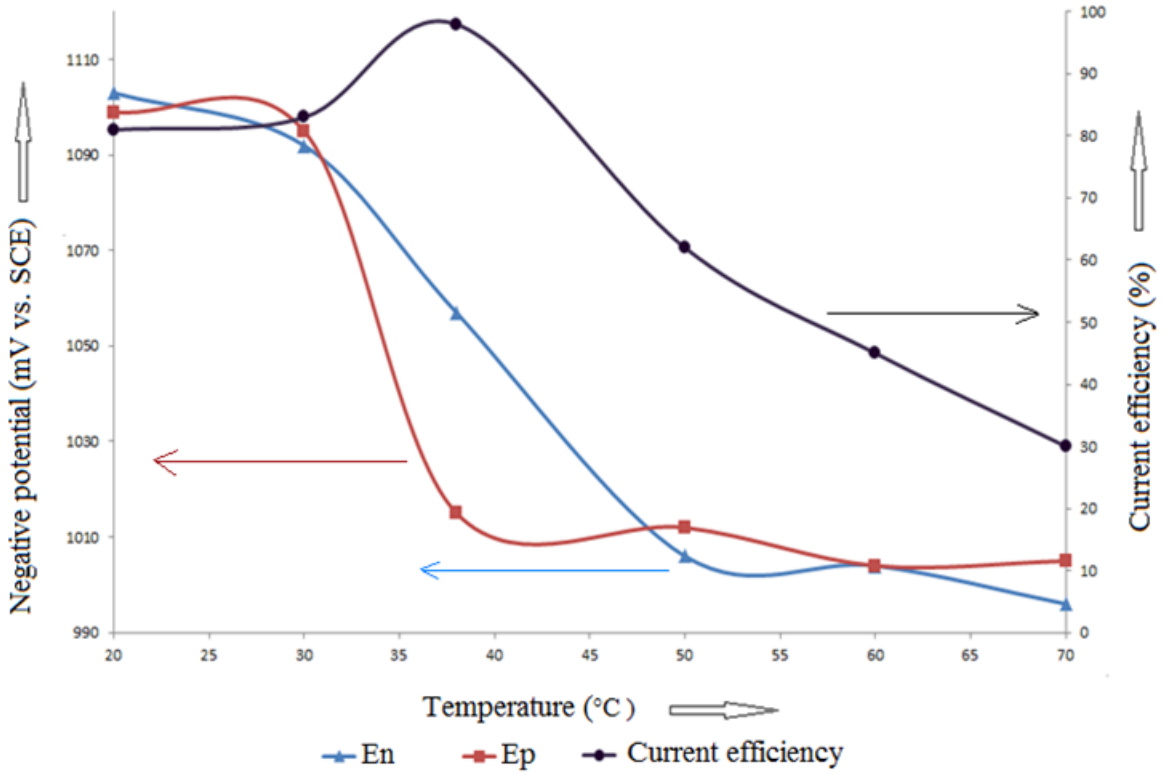

Figure 4.8. Influence of temperature on the nucleation and plating potentials as well as the current efficiency for a solution containing 50 gL^{-1} zinc and 150 gL^{-1} H_2SO_4. Arrows on graphs indicate which scale to use.

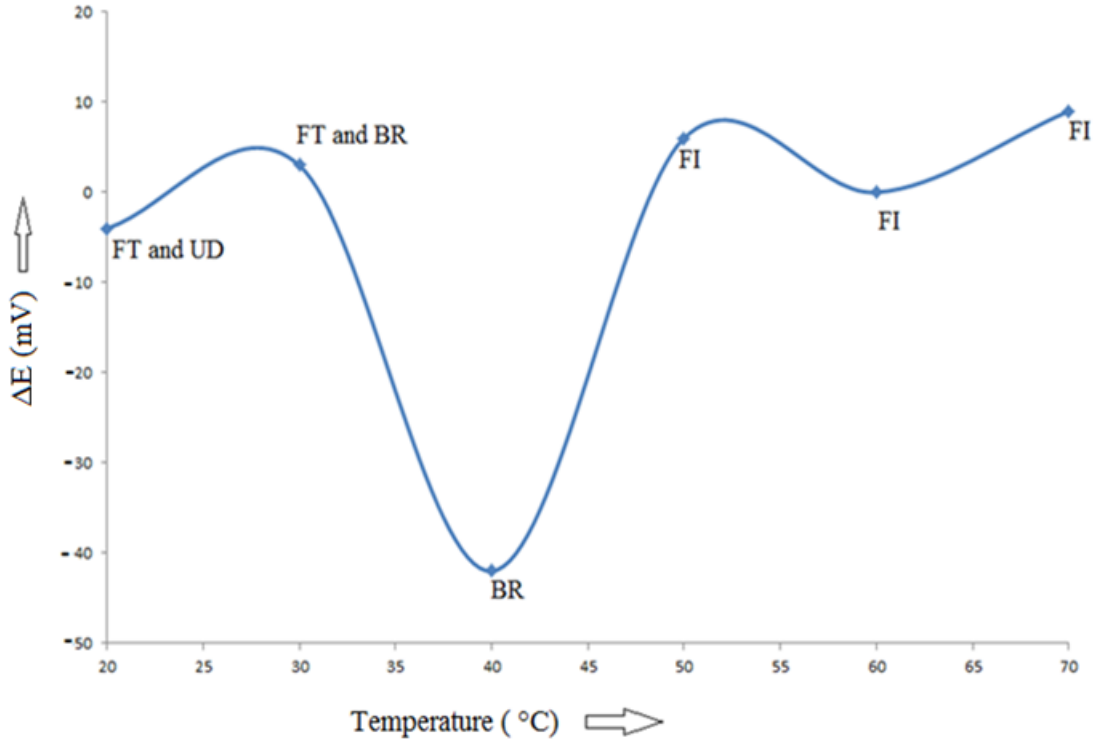

Figure 4.9. Variation of the difference between nucleation and plating potentials with temperature for a solution containing 50 gL^{-1} zinc and 150 gL^{-1} sulphuric acid.

4.4.4 Potassium permanganate additions

The results given in figure 4.10 and figure 4.11 indicates that potassium permanganate has a very significant effect on the nucleation and plating potentials with a significant move to more positive potentials up to concentrations of about 40 mgL^{-1} which then stabilizes to a relatively constant value at higher concentrations. The move to more positive potentials is not unexpected with the introduction of an additional reducible species into the electrolyte as is the larger increase in the nucleation potential which should be more sensitive to such an addition at low concentrations. The shift in the plating potential to more positive potentials is surprising in view of the high current density used and at which the current contribution of the permanganate reduction would be relatively small indicating that the effect of the permanganate on the plating process is probably indirect. This is also supported by the relatively small influence of the permanganate on the current efficiency. Nonetheless, the results confirm that if artificial solutions are to be used to simulate plant electrolytes permanganate should be added if comparable results with those of plant solutions are to be obtained.

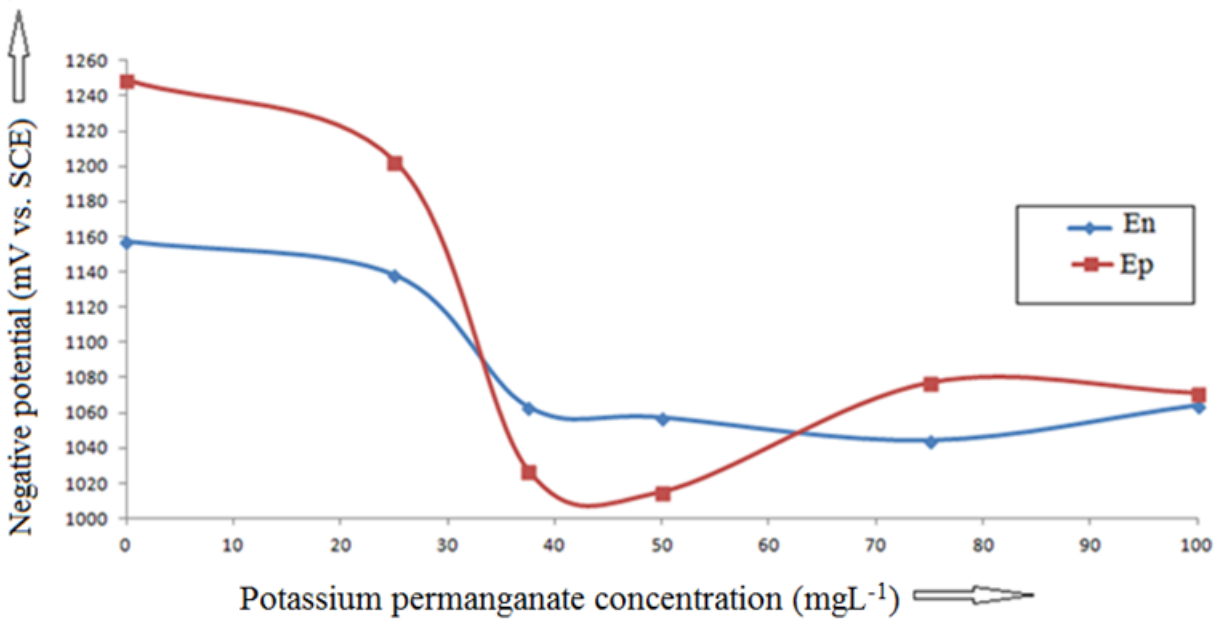

Figure 4.10. Influence of the potassium permanganate concentration on the nucleation and plating potentials for a solution containing 50 gL^{-1} zinc, 150 gL^{-1} H_2SO_4 at 38 ^0C.

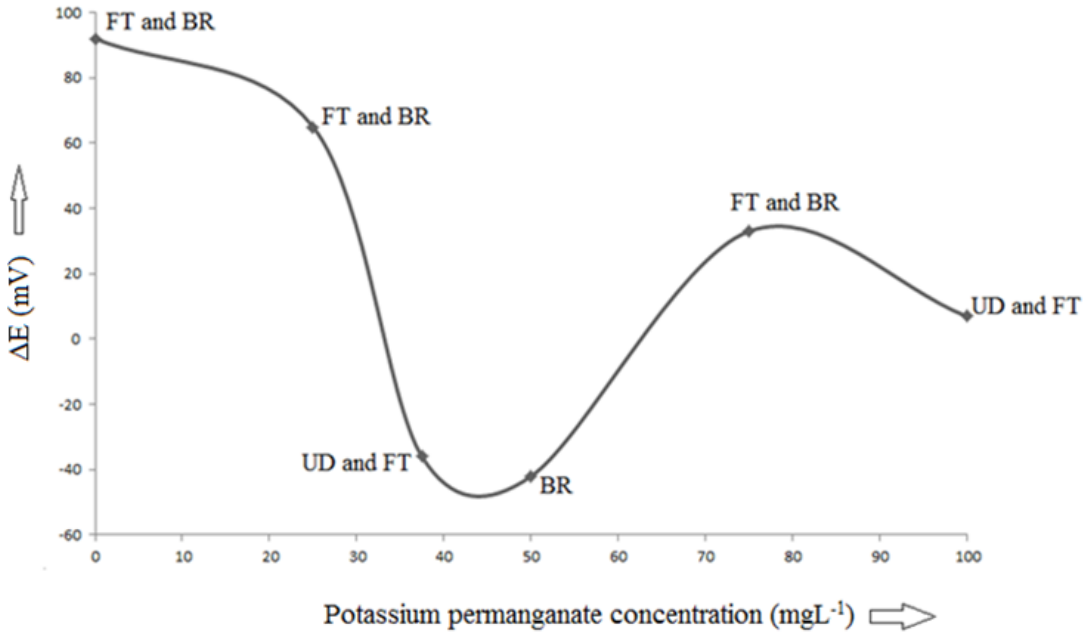

Figure 4.11. Variation of the difference between nucleation and plating potentials with potassium permanganate concentrations for a solution containing 50 gL^{-1} zinc and 150 gL^{-1} sulphuric acid at 38 ^{0}C.

4.5 Additives

The role of additives, such as grain refiners and levellers, in electrowinning zinc from zinc sulphate electrolytes was also evaluated using the galvanodynamic technique. The grain refiners evaluated were saccharin and tetrabutylammonium bromide, and the levellers, pyridine and butyne-1, 4, diol. The grain refiners and levellers seem to be very specific in their mode of inhibition of nucleation and plating potentials. Generally all the additives tested inhibited both nucleation and plating potentials, as expected, and as will be discussed in more detail in the following sections.

4.5.1 Grain refiners

4.5.1.1 Saccharin additions

The influence of saccharin on the nucleation and plating potentials are shown in figure 4.12 indicating that saccharin moves both the nucleation and plating potentials to more negative values, as would be expected, but then unexpectedly moves the nucleation potential first to more positive

values and then again to more negative values, but mostly still more positive than the plating potentials. These tendencies are summarized in the potential difference diagram shown as figure 4.13, and when considered together with the structure data indicates that control of saccharin additions may be problematic as good quality plated zinc is only obtained in a small concentration window.

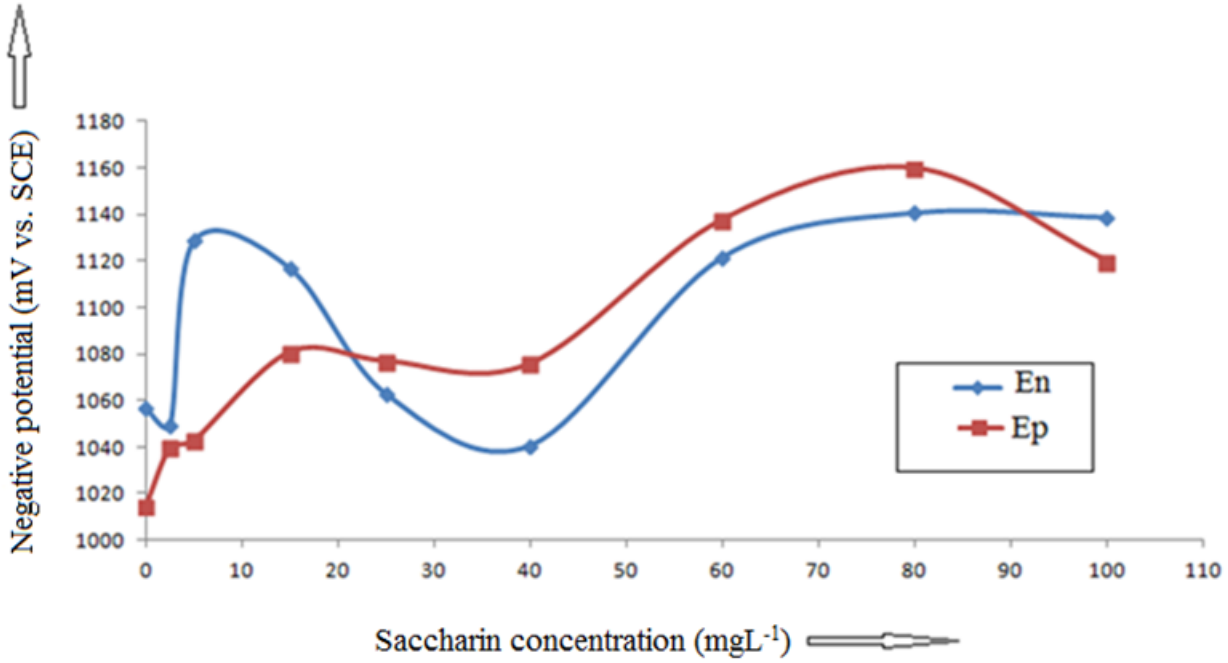

Figure 4.12. Influence of the saccharin additions on the nucleation and plating potentials for a solution containing 50 gL^{-1} zinc, 150 gL^{-1} H_2SO_4 at 38 ^0C.

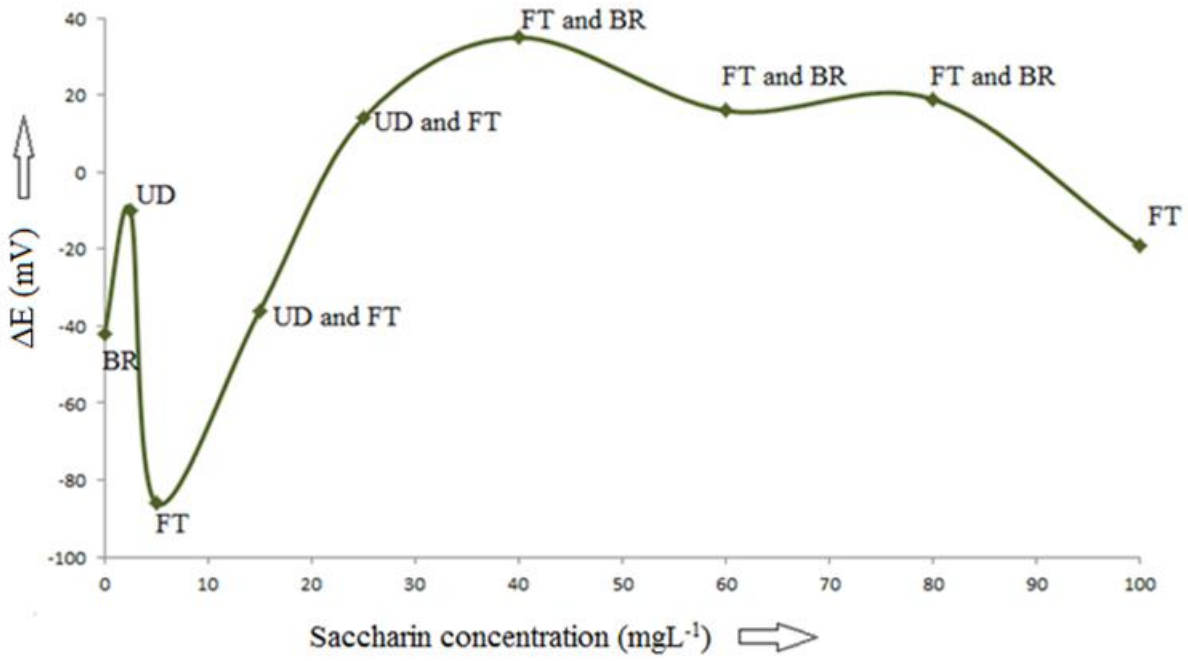

Figure 4.13. ΔE as a function of saccharin additions to a solution containing 50 gL^{-1} zinc, 150 gL^{-1} sulphuric acid at 38 ^{0}C.

4.5.1.2 Tetrabutylammonium bromide additions

The results obtained for the tetrabutylammonium bromide show similar trends to those for saccharin but with nucleation and plating potentials very close to each other, as indicated in figures 4.14 and 4.15. From this it can be predicted that good quality zinc should be obtained at all concentrations evaluated, as was indeed found to be the case. The relatively wide concentration range in which good quality deposits is obtained indicates that it may potentially be a better additive than saccharin.

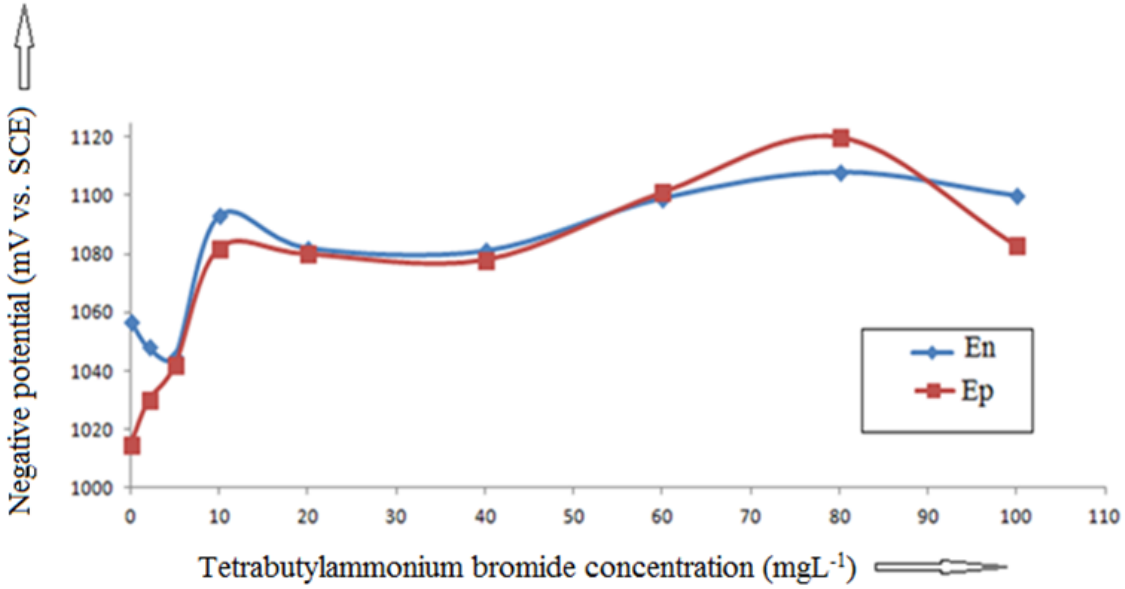

Figure 4.14. Influence of the tetrabutylammonium bromide additions on the nucleation and plating potentials for a solution containing 50 gL^{-1} zinc, 150 gL^{-1} H_2SO_4 at 38 ^0C.

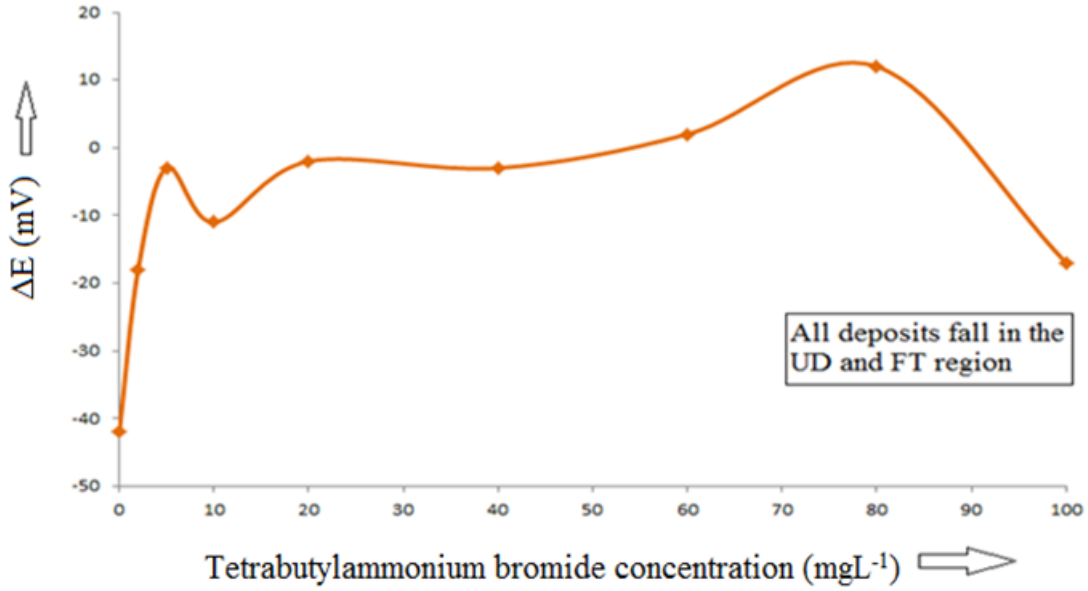

Figure 4.15. Variation of the difference between nucleation and plating potentials with tetrabutylammonium bromide additions to a solution containing 50 gL^{-1} zinc, 150 gL^{-1} sulphuric acid at 38 ^{0}C.

4.5.2 Levellers

4.5.2.1 Pyridine additions

The results shown in figures 4.16 and 4.17 indicate that the pyridine inhibits both nucleation and plating to about the same extent by moving both the nucleation and plating potentials at low concentrations, which after a slight movement to more positive potentials do not change significantly with further additions. Pyridine thus has a wide range of concentration where its ΔE is steady and optimum levelness can be obtained. However, the quality of the deposits become unsatisfactory at high concentrations, i.e. higher than 70 mgL^{-1}, which is not clearly predicted by the change in nucleation and plating potentials although the difference between the potentials becomes smaller at these concentrations.

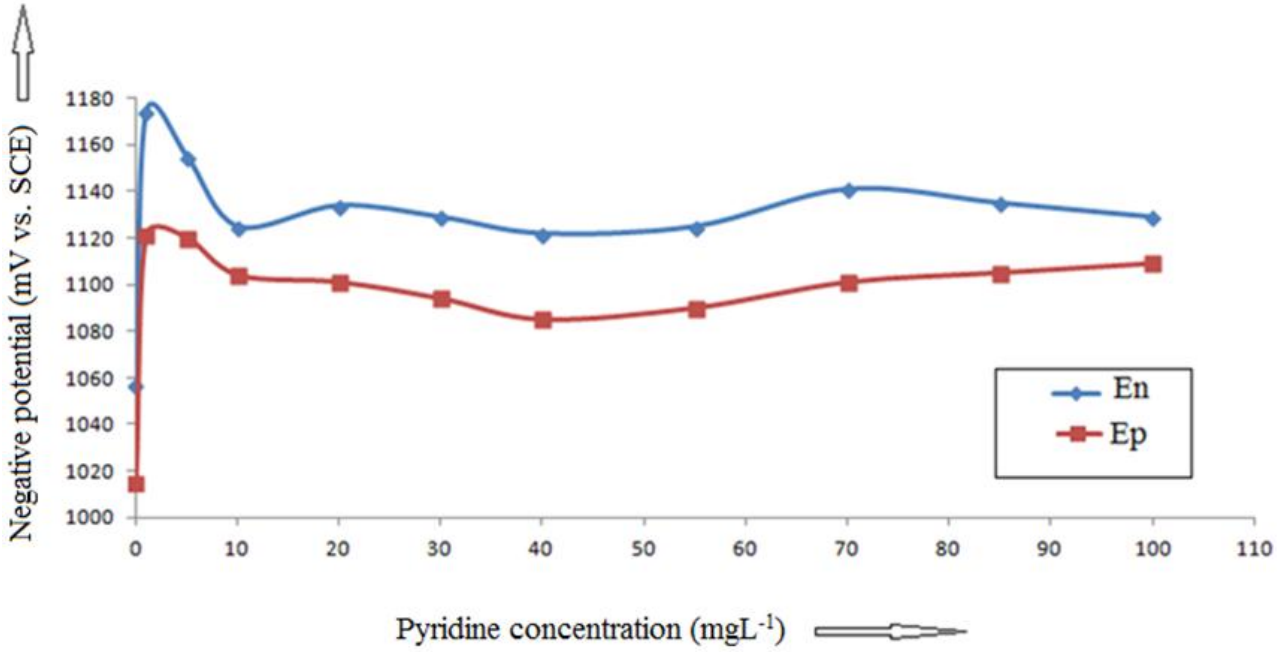

Figure 4.16. Influence of the pyridine additions on the nucleation and plating potentials to a solution containing 50 gL^{-1} zinc, 150 gL^{-1} H_2SO_4 at 38 ^0C.

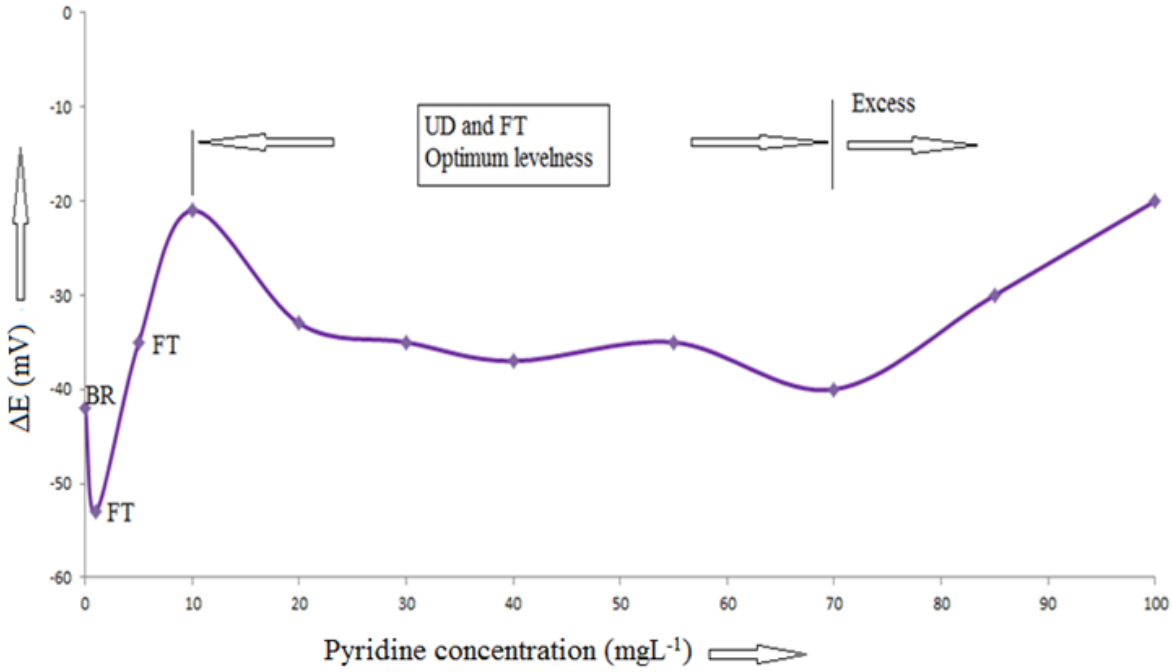

Figure 4.17. Variation of the difference between nucleation and plating potentials with pyridine concentrations for a solution containing 50 gL^{-1} zinc, 150 gL^{-1} sulphuric acid at 38 ^0C.

4.5.2.2 Butyne-1, 4, diol addition

The results shown in figures 4.18 and 4.19 indicate that the butyne-1, 4, diol additions also inhibit both nucleation and plating at low concentrations, with the nucleation potential staying relatively constant while the plating potential becomes more positive at intermediate potentials and then more negative at higher potentials. The structure of the plated metal is rather unpredictable at low concentrations but acceptable structures are obtained at intermediate and high concentrations. These results indicate that it would indeed be difficult to predict the structure of the plated metal by only using the difference between the nucleation and plating potentials.

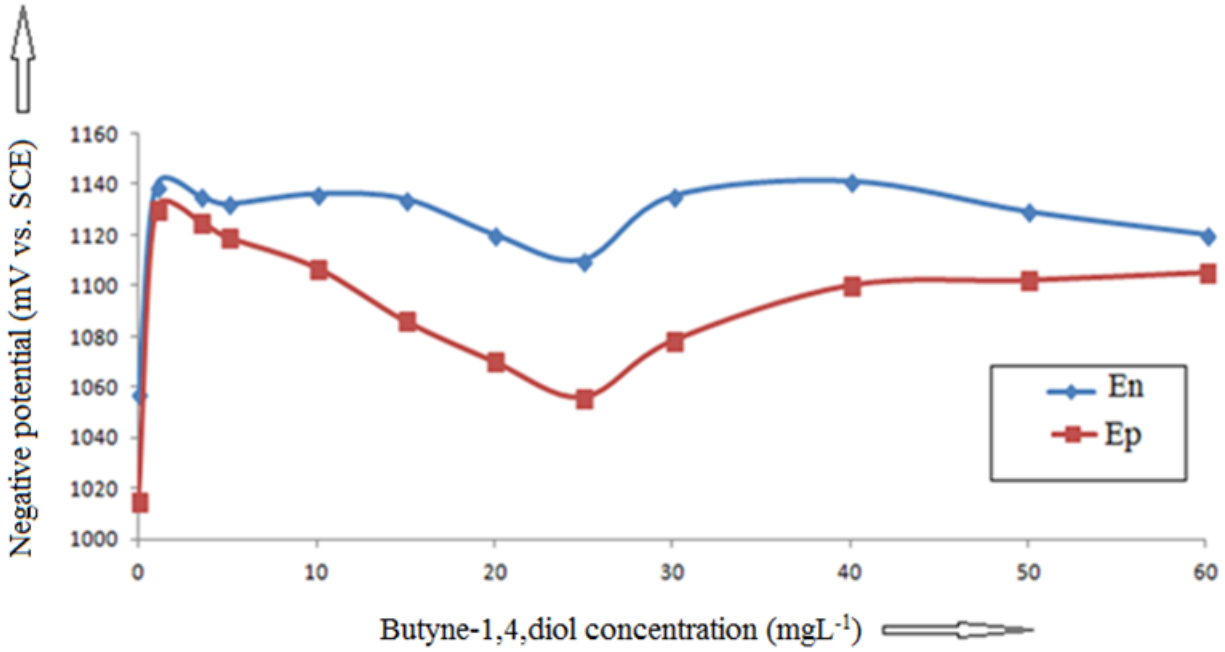

Figure 4.18. Influence of butyne-1, 4, diol additions on the nucleation and plating potentials for a solution containing 50 gL^{-1} zinc, 150 gL^{-1} H_2SO_4 at 38 ^0C.

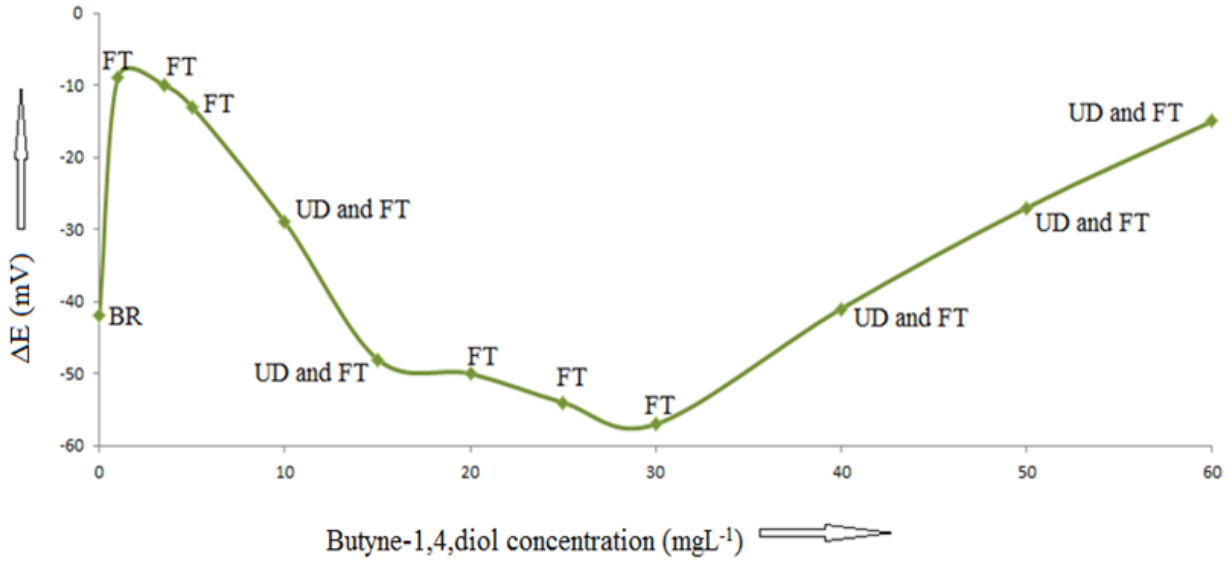

Figure 4.19. Variation of the difference between nucleation and plating potentials with butyne-1,4,diol additions to a solution containing 50 gL^{-1} zinc, 150 gL^{-1} sulphuric acid at 38 ^{0}C.

The main action mechanisms of grain refiners seem to involve the nucleation process and those of levellers seem control the growth process. The potential difference ΔE is useful for selecting a grain refiner but not for selecting a levelling agent. This rather limits the usefulness of the Adcock diagram for the evaluation of additives for zinc electrowinning from sulphate electrolytes.

5 CONCLUSIONS

The present work indicates that galvanodynamic polarization measurements may be useful to predict the nature of the metal that will be plated from acidic aqueous zinc sulphate electrolytes using the measured nucleation and plating potentials. The two scan rate galvanodynamic technique for measuring polarization potentials developed in this work had good repeatability and has demonstrated its usefulness as a reliable tool for measuring nucleation and plating potentials. The reproducibility and relevance of all nucleation and plating potential measurements strongly depended on strict adherence to substrate surface preparation methods and procedures. It was also important to maintain strict repeatability of electrolytes and plating conditions as very small changes were found to influence potential measurements.

It was found necessary to compensate for the solution resistance which contributes significantly to the potential inherent in the measured plating potentials at a relatively high current density of 600 Am^{-2}. Frequency response analysis was found to be a repeatable and reliable technique for measuring the solution resistance responsible for the IR-drop measurement error. It was also observed that conductivity measurements and model approximations from literature were also convenient and reliable methods for estimating this resistance without significant error.

A relationship was confirmed between the difference between nucleation and plating potentials and grain structure. The relationship was not absolute but was useful in predicting the structure of plated zinc deposits in practical ranges typically used in industrial zinc plating. However it was clear that it may be an oversimplification to conclude that three dimensional nucleation is favoured over growth if the plating potential is more negative than the plating potential. The results showed that UD deposits were rather obtained for ΔE values around zero with FT and BR type deposits obtained at more positive as well as negative values.

A unique range in terms of the difference in the nucleation and plating potentials and the plating potential was identified where a high probability of plating good quality zinc deposits was possible. Such a range should be useful to guide remedial action following industrial upsets.

The influence of temperature on the plating characteristics was not substantial at both low and high temperatures which led to the conclusion that the approach to characterise zinc plating by polarization characteristics is probably not valid for conditions where significant rates of hydrogen ion reduction occur.

The study on grain refiners and levellers indicated that grain refiners affect the nucleation process while levellers control the growth process. The potential difference ΔE should be useful for identifying and predicting grain refinement but not as useful as in the case with levelling. This limits the utility of the polarization parameter diagram as proposed by Adcock for the evaluation of additives for zinc electrowinning from sulphate electrolytes.

6 RECOMMENDATIONS AND FUTURE WORK

The proposed model could still be improved in many ways. It was noted in the evaluation of the plated zinc that the nature of the plated metal changes at some stage during the plating without any apparent cause. This change is not reflected in the data generated in this study. It could be a good idea to further investigate this.

In the present work reference was made to the types of structures (BR, UD and FT) on a qualitative basis and the determination of the structure may be somewhat subjective. Getting reliable results was difficult in practice, because in many cases, the deposit was initially made up of a large number of small crystallites at the surface of the substrate and some three-dimensional nucleation was observed. Then, after a deposit thickness which could range from a fraction of a micrometre to about 25 μm the structure changed. However, even in this latter part of some deposits, a transition appeared between a BR and FT structure, and a UD-FT texture. This is presumably because initial deposits should occur at the energetically most preferred sites while later, when the polarization is higher, this effect will no longer dominate. Exclusion zones may also form around deposits due to IR-drop considerations. Due to these problems of discerning between the structures more reliable methods are required to help determine the type of deposit structure on a more quantitative basis such as a metallographic image analysis program capable of processing the data to yield practically useful results.

Programmes such as Automatic Image Analysis may be recommended which improve the image to aid the analysis system by developing a methodical interpretation of images and their contents. (Syrjauo, 2008). This may be useful for purposes where the plated metal is the end product and modelling is required. However, in the case of zinc electrowinning it may be a better idea to rather concentrate on practically useful measures such as the chemical analysis for purity and mechanical properties such as ductility, adhesion and compactness of the deposits as the metal is seldom if ever functionally used in the as produced state.

In the present study the correlationships between polarization parameters and deposit structure were done on 80 minute deposits. This is a very short time compared to the practical plating times used in industrial zinc electrowinning. It may be a good idea to evaluate the validity of the correlations for longer plating times similar to those used practically.

7 REFERENCES

Adcock, P., Adeloju, S., and Newman, O. (2002). Measurement of polarization parameters impacting on electrodeposit morphology I: Theory and development of technique. Journal of Applied Electrochemistry, 32, 1101 - 1107.

Adcock, P., Quillinan, A., Clark, B., Newman, O., and Adeloju, S. (2004). Measurement of polarization parameters impacting on electrodeposit morphology. II:conventional zinc electrowinning solutions. Journal of Applied Electrochemistry, 34, 771 - 780.

Andersen, T., Kerby, R., and O'Keefe, T. (1985). Control techniques for industrial electrodeposition from aqueous solutions. Journal of Metals, 37, 36 - 43.

Barton, G., and Scott, A. (1992). A validated mathematical model for a zinc electrowinning cell. Journal of Applied Electrochemistry, 104 - 115.

Bockris, J., Reddy, A., and Gamboa-Aldeco, M. (2000). The electrogrowth of metals on electrodes. Modern Electrochemistry, 2A, 2nd Edition, 1293 – 1347.

Bond, A. M. (1999). 200 years of practical electroanalytical chemistry: Determination of trace metals in zinc plant electrolyte by voltammetric and potentiometric techniques. Analytical Chimica Acta, 400, 333 - 379.

Budevski, E., Staikov, G., and Lorenz, W. (2000). Electrocrystallization; Nucleation and growth phenomena. Electrochemica Acta(45), 2559 - 2574.

Epelboin, I., Ksouri, M., and R, W. (1975). On a model for the electrocrystallization of zinc involving an autocatalytic step. Journal of the Electrochemical Society(122(9)), 1206 - 1214.

Fischer, H. (1954). Elektrolytische Abscheidung und Elektrokristallisation van Metallen. Springer Verlag, 729.

Gabrielli, C. (1998). Identification of electrochemical processes by frequency response analysis. 3, 1 - 23.

Gonzalez-Dominguez, J. (1994). A review of lead and zinc electrodeposition control by polarization techniques. Minerals engineering, 7(1), 87-97.

Guillaume, P., Leclerc, N., Boulanger, C., Lecuire, J., and Lapicque, F. (2007). Investigation of optimal conditions for zinc electrowinning from aqueous sulpfuric acid electrolytes. Journal of Applied Electrochemistry, 37, 1237 - 1243.

Gurmen, S., and Emre, M. (2003). A laboratory-scale investigation of alkaline zinc electrowinning. Minerals Engineering, 16(6), 559 - 569.

Han, J., and O'Keefe, T. (1992). The degradation of aluminium cathodes by fluoride ion during zinc electrowinning. Journal of Applied Electrochemistry, 22, 606 - 612.

Hosny, A., O'Keefe, T., and James, W. (1989). Hull cell technique for evaluating zinc sulfate electrolytes. Minerals Engineering, 2(3), 415.

Ivanov, I., and Stefanov, Y. (2002). Electroextraction of zinc from sulphate electrolytes containing antimony and hydroxyethylated-butayne-2-diol2,4: Part 3. The influence of manganese ions and a divided cell. Hydrometallurgy, 64, 181 - 186.

Jin, S., and Ghali, E. (2001). Effects of gelatine , thiourea and chloride ion on the copper cathode polarization behaviour in acidic copper sulphate at 65 degrees celcius. Canadian Metallurgical Quarterly, 40(4), 433 - 439.

Kalantary, M. R., and Gabe, D. (1993). Unipolar and bipolar pulsed current electrodeposition for PCB production. Journal of Applied Electrochemistry, 23, 231 - 240.

Kauffiman, A. (1997). Understanding electrochemical cells. Solartron Instruments, 15 - 30.

Kelsall, G., Guerra, E., Li, G., and Bestetti, M. (2000). Effects of manganese(II) and chloride ions in zinc electrowinning reactors. In Proceedings of Electrochemical Society, 14, 350 - 361.

Kerby, R. (1984). US Patent 4 443 301.Washington, DC: U.S. Patent and Trademark Office.

Kerby, R. C., and Jackson, H. E. (1978). Organic levelling agents for electrolytic refining of lead. Canadian Metallurgical Society, Q 17, 125 - 131.

Kerby, R., Jackson, H., O'Keefe, T., and Wang, Y. (1977). Evaluation of organic additives for use in zinc electrowinning. Metallurgical Transactions B, 8B, 661 - 612.

Lafront, S., Veilleux, B., and Ghali, E. (2002). Galvanostatic and microscopic studies of nodulation during copper electrolysis. Journal of Applied Electrochemistry, 32, 329 - 337.

Lee, M. G., and Jorne, J. (1992). On the kinetic mechanism of zinc electrodeposition in the region of negative polarization resistance. Journal of Electrochemical Society, 139, 2841 - 2844.

Liu, H., Favier, F., Ng, K., Zach, M. P., and Penner R, M. (2001). Size selective electrodeposition of meso-cale metal particles: a general method. Electrochim Acta, 671 - 677.

Mackinnon, D. J., and Brannen, J. M. (1977). Zinc deposit structures obtained from high purity synthetic and industrial acid sulphate electrolytes with and without antimony and glue additions. Journal of Applied Electrochemistry, 7, 451 - 459.

Mackinnon, D. J., Morrison, R. M., and Brannen, J. M. (1985). The effects of nickel and cobalt and their interaction with antimony on zinc electrowinning from industrial acid sulphate electrolyte. Journal of Applied Electrochemistry, 16, 53 - 61.

Mackinnon, D., Brannen, J., and Fenn, P. (1987). Characterisation of impurity effects in zinc electrowinning from industrial acid sulphate electrolyte. Journal of Applied Electrochemistry, 17, 1129 - 1143.

Nichols, R. J., and Kolb, D. M. (1991). STM observations of the initial stages of copper deposition on gold single-crystal electrodes. Journal of Electroanalytical Chemistry, 313, 109 - 119.

Oniciu, L., Muresan, L., Topan, V. A., Pantea, A., and Ghertoiu, D. (1986). Metal Electrodeposition. IV, 545.

Paunovic, M., and Schlesinger, M. (2006). Fundamentals of electrodeposition. Wiley, 2nd Edition, 214.

Rashidi, A. M., and Amadeh, A. (2010). Effect of electroplating parameters on microstructure of nanocrystalline nickel coatings. Journal of Materials Science Technology, 82 - 86.

Robinson, D., and O'Keefe, T. (1976). Effects of antimony and glue on zinc electrocrystallization behaviour. Journal of Applied Electrochemistry, 6, 1 - 7.

Rodrgues, J. M., and O, M. E. (1995). Improving performance of anodes for zinc electrowinning. The Minerals, Metals and Materials Society, 163.

Saber, K., Koch, C., and Fedkiw, P. (2003). Pulse current electrodeposition of nanocrystalline zinc. Materials Science and Engineering, A 341, 174 - 181.

Scientific, T. F. (2014). Measuring the conductivity of pure water. Retrieved May 12, 2015, from Google: http://www.thermoscientific.com/content/

Scott, A., Pitblado, R., Barton, G., and Ault, A. R. (1988). Experimental determination of the factors affecting zinc electrowinning efficiency. Journal of Applied Electrochemistry(18), 120-127.

Staikov, G. (2007). Electrocrystallization in nanotechnology. Wiley, 16 - 18.

Syrjauo, M. (2008). Automatic Image Analysis. Retrieved March 26, 2014, from Google: http://www.space.fmi.fi/graduateschool/Lectures08/

Tripathy, B. C., S.C, D., Singh, P., and Hefter, G. (1999). Zinc electrowinning from acidic sulphate solutions. Part III: Effects of quartenary ammoniun bromides. Journal of Applied Electrochemistry, 29, 1229 - 1235.

Troyon, M., Darrort, V., Ebothe, J., Bissieux, C., and C, N. (1995). Qauntitative study by atomic force microscopy and spectrophotometry of the roughness and brightness of electrodeposited nickel in the presence of additives. Thin Solid Films, 265(1 - 2), 52 - 57.

Van Dyk, J. P. (2006). An Overview of the Zincor Process. The Journal of the Southern African Institute of Mining and Metallurgy, 280.

Venkateswaran, K., Srinivasaran, G. N., and Nandakumar, V. (1996). Electrowinning of zinc - effect of metallic impurities and addition agents. Bulletin of Electrochemistry, 12, 349 - 351.

Voss, G., and Hoffman, H. (1975, November 18). Patent No. United States Patent. US 3920528A. Berlin, Germany.

Wark, I. W. (1979). The electrodeposition of zinc from acidified zinc sulphate solution. Journal of Applied Electrochemistry, 9, 721 - 730.

Warren, I. H. (1985). The application of polarization measurements in the control of zinc tankhouse operation. Zinc '85 .Proceedings of International Symposium on Extractive Metallurgy of Zinc, 16, 251 - 264.

Winand, R. (1992). Electrocrystallization: theory and applications. Hydrometallurgy, 29, 567 - 598.

Winand, R. (1994). Electrodeposition of metals and alloys - new results and perspectives. Electrochimica Acta, 39(8/9), 1091 - 1105.

8 APPENDICES

Appendix A. Nucleation potential measurements

[Zn] (gL^{-1})	[H_2SO_4] (gL^{-1})	Temperature (^0C)	Additive (mgL^{-1})	En (mV vs. SCE) 1	2	3	Mean	(mV) Standard deviation
10	150	38	None	-1101	-1106	-1105	-1104	3
30	150	38	None	-1092	-1086	-1091	-1090	3
40	150	38	None	-1075	-1080	-1079	-1078	3
60	150	38	None	-1086	-1089	-1091	-1089	3
80	150	38	None	-1078	-1072	-1074	-1075	3
90	150	38	None	-1032	-1038	-1034	-1035	3
100	150	38	None	-1053	-1047	-1049	-1050	3
120	150	38	None	-1035	-1034	-1032	-1033	2
50	0	38	None	-1059	-1055	-1052	-1055	4
50	10	38	None	-1088	-1094	-1092	-1092	3
50	50	38	None	-1076	-1083	-1081	-1080	4
50	100	38	None	-1073	-1078	-1074	-1075	3
50	200	38	None	-1089	-1094	-1091	-1091	3
50	250	38	None	-1079	-1080	-1086	-1083	4
50	150	20	None	-1101	-1105	-1102	-1103	2
50	150	30	None	-1095	-1090	-1091	-1092	3
50	150	40	None	-1053	-1060	-1057	-1057	4
50	150	50	None	-1004	-1011	-1005	-1006	4
50	150	60	None	-1001	-1008	-1004	-1004	4
50	150	70	None	-992	-1001	-996	-996	5
			TBABr					
50	150	38	2	-1045	-1052	-1046	-1048	4
50	150	38	5	-1042	-1048	-1046	-1045	3
50	150	38	10	-1091	-1095	-1094	-1093	2
50	150	38	40	-1084	-1082	-1078	-1081	3
50	150	38	100	-1098	-1105	-1097	-1100	4

Appendix A. Continued

[Zn]	$[H_2SO_4]$	Temperature	Additive	En				
				(mV vs. SCE)				(mV)
(gL^{-1})		(^0C)	(mgL^{-1})	1	2	3	Mean	Standard deviation
			Saccharin					
50	150	38	2.5	-1048	-1052	-1049	-1050	2
50	150	38	5	-1126	-1132	-1130	-1129	3
50	150	38	15	-1114	-1122	-1116	-1117	4
50	150	38	25	-1062	-1066	-1062	-1063	2
50	150	38	40	-1039	-1045	-1040	-1041	3
50	150	38	60	-1118	-1123	-1124	-1122	3
50	150	38	80	-1139	-1145	-1138	-1141	4
50	150	38	100	-1135	-1141	-1140	-1139	3
			Pyridine	0	0	0		
50	150	38	1	-1178	-1173	-1172	-1174	3
50	150	38	5	-1150	-1157	-1159	-1155	5
50	150	38	10	-1127	-1123	-1126	-1125	2
50	150	38	20	-1136	-1135	-1132	-1134	2
50	150	38	30	-1125	-1132	-1129	-1129	4
50	150	38	40	-1119	-1123	-1125	-1122	3
50	150	38	55	-1128	-1122	-1126	-1125	3
50	150	38	70	-1146	-1140	-1138	-1141	4
50	150	38	85	-1138	-1132	-1136	-1135	3
50	150	38	100	-1126	-1134	-1126	-1129	5
			Pyridine; Saccharin					
50	150	38	10;100	-1184	-1190	-1188	-1187	3
50	150	38	40;40	-1155	-1146	-1151	-1151	5

Appendix A. Continued

[Zn] (gL^{-1})	[H_2SO_4] (gL^{-1})	Temperature (^0C)	Additive (mgL^{-1})	En (mV vs. SCE) 1	2	3	Mean	(mV) Standard deviation
			Butyne-1,4,diol					
50	150	38	1	-1140	-1136	-1142	-1139	3
50	150	38	3.5	-1139	-1132	-1135	-1135	4
50	150	38	5	-1130	-1134	-1133	-1132	2
50	150	38	10	-1133	-1140	-1136	-1136	4
50	150	38	15	-1131	-1134	-1138	-1134	4
50	150	38	20	-1118	-1124	-1119	-1120	3
50	150	38	25	-1114	-1108	-1109	-1110	3
50	150	38	30	-1134	-1139	-1133	-1135	3
50	150	38	40	-1145	-1143	-1136	-1141	5
50	150	38	50	-1131	-1132	-1125	-1129	4
50	150	38	60	-1118	-1119	-1124	-1120	3
			$KMnO_4$					
50	150	38	25	-1140	-1134	-1139	-1138	3
50	150	38	37.5	-1060	-1067	-1063	-1063	4
50	150	38	50	-1061	-1056	-1055	-1057	3
50	150	38	75	-1042	-1046	-1045	-1044	2
50	150	38	100	-1060	-1068	-1065	-1064	4

Appendix B. Plating potential measurements

[Zn] (gL^{-1})	[H_2SO_4] (gL^{-1})	Temperature (^0C)	Additive (mgL^{-1})	Ep measured (mV vs. SCE) 1	2	3	IRs (mV)	Ep corrected (mV vs. SCE) 1	2	3	Mean	Standard deviation (mV)
10	150	38	None	-1167	-1172	-1168	-55	-1112	-1117	-1113	-1114	3
30	150	38	None	-1131	-1135	-1134	-62	-1069	-1073	-1072	-1071	2
40	150	38	None	-1127	-1134	-1133	-67	-1060	-1067	-1066	-1064	4
60	150	38	None	-1114	-1120	-1116	-72	-1042	-1048	-1044	-1045	3
80	150	38	None	-1109	-1102	-1103	-73	-1036	-1029	-1030	-1032	4
90	150	38	None	-1097	-1103	-1099	-83	-1014	-1020	-1016	-1017	3
100	150	38	None	-1145	-1140	-1144	-88	-1057	-1052	-1056	-1055	3
120	150	38	None	-1132	-1137	-1134	-98	-1034	-1039	-1036	-1036	3
50	0	38	None	-1609	-1602	-1604	-614	-995	-988	-990	-991	4
50	10	38	None	-1372	-1379	-1374	-422	-950	-957	-952	-953	4
50	50	38	None	-1245	-1244	-1241	-176	-1069	-1068	-1065	-1067	2
50	100	38	None	-1125	-1132	-1130	-95	-1030	-1037	-1035	-1034	4
50	200	38	None	-1081	-1074	-1082	-59	-1022	-1015	-1023	-1020	4
50	250	38	None	-1065	-1073	-1068	-52	-1013	-1021	-1016	-1017	4
50	150	20	None	-1178	-1183	-1176	-80	-1098	-1103	-1096	-1099	4
50	150	30	None	-1166	-1170	-1172	-74	-1092	-1096	-1098	-1095	3
50	150	40	None	-1091	-1085	-1089	-73	-1018	-1012	-1016	-1015	3
50	150	50	None	-1076	-1069	-1074	-61	-1015	-1008	-1013	-1012	4
50	150	60	None	-1054	-1062	-1058	-54	-1000	-1008	-1004	-1004	4
50	150	70	None	-1048	-1055	-1053	-47	-1001	-1008	-1006	-1005	4

Appendix B. Continued

[Zn]	$[H_2SO_4]$	Temperature	Additive	Ep measured			IRs	Ep corrected				
(gL^{-1})		(^0C)	(mgL^{-1})	(mV vs. SCE)			(mV)	(mV vs. SCE)				(mV)
				1	2	3		1	2	3	Mean	Standard deviation
			TBABr									
50	150	38	2	-1096	-1090	-1092	-64	-1032	-1026	-1028	-1029	3
50	150	38	5	-1109	-1105	-1103	-64	-1045	-1041	-1039	-1042	3
50	150	38	10	-1143	-1148	-1146	-64	-1079	-1084	-1082	-1082	3
50	150	38	40	-1146	-1142	-1141	-65	-1081	-1077	-1076	-1078	3
50	150	38	100	-1152	-1146	-1150	-66	-1086	-1080	-1084	-1083	3
			Saccharin									
50	150	38	2.5	-1101	-1108	-1103	-64	-1037	-1044	-1039	-1040	4
50	150	38	5	-1106	-1105	-1111	-64	-1042	-1041	-1047	-1043	3
50	150	38	15	-1147	-1141	-1146	-64	-1083	-1077	-1082	-1081	3
50	150	38	25	-1139	-1145	-1140	-64	-1075	-1081	-1076	-1077	3
50	150	38	40	-1136	-1143	-1140	-64	-1072	-1079	-1076	-1076	4
50	150	38	60	-1199	-1206	-1201	-64	-1135	-1142	-1137	-1138	4
50	150	38	80	-1226	-1220	-1228	-65	-1161	-1155	-1163	-1160	4
50	150	38	100	-1183	-1190	-1186	-66	-1117	-1124	-1120	-1120	4

Appendix B. Continued

[Zn]	$[H_2SO_4]$	Temperature	Additive	Ep measured			IRs	Ep corrected				
(gL^{-1})		(^0C)	(mgL^{-1})	(mV vs. SCE)			(mV)	(mV vs. SCE)				(mV)
				1	2	3		1	2	3	Mean	Standard deviation
			Pyridine									
50	150	38	1	-1186	-1190	-1184	-66	-1120	-1124	-1118	-1121	3
50	150	38	5	-1183	-1191	-1185	-66	-1117	-1125	-1119	-1120	4
50	150	38	10	-1174	-1169	-1168	-66	-1108	-1103	-1102	-1104	3
50	150	38	20	-1170	-1164	-1168	-66	-1104	-1098	-1102	-1101	3
50	150	38	30	-1155	-1161	-1158	-65	-1090	-1096	-1093	-1093	3
50	150	38	40	-1148	-1154	-1152	-66	-1082	-1088	-1086	-1085	3
50	150	38	55	-1153	-1159	-1157	-66	-1087	-1093	-1091	-1090	3
50	150	38	70	-1164	-1171	-1167	-66	-1098	-1105	-1101	-1101	4
50	150	38	85	-1168	-1173	-1173	-66	-1102	-1107	-1107	-1105	3
50	150	38	100	-1179	-1173	-1173	-66	-1113	-1107	-1107	-1109	3
			Pyridine; Saccharin									
50	150	38	10;100	-1226	-1231	-1216	-68	-1158	-1163	-1148	-1156	8
50	150	38	40;40	-1250	-1256	-1251	-67	-1183	-1189	-1184	-1185	3

Appendix B. Continued

[Zn]	[H_2SO_4]	Temperature	Additive	Ep measured			IRs	Ep corrected				
(gL^{-1})		(^0C)	(mgL^{-1})	(mV vs. SCE)			(mV)	(mV vs. SCE)				(mV)
				1	2	3		1	2	3	Mean	Standard deviation
			Butyne-1,4,diol									
50	150	38	1	-1193	-1199	-1196	-66	-1127	-1133	-1130	-1130	3
50	150	38	3.5	-1190	-1194	-1189	-66	-1124	-1128	-1123	-1125	3
50	150	38	5	-1182	-1188	-1188	-67	-1115	-1121	-1121	-1119	3
50	150	38	10	-1170	-1177	-1175	-67	-1103	-1110	-1108	-1107	4
50	150	38	15	-1149	-1155	-1152	-66	-1083	-1089	-1086	-1086	3
50	150	38	20	-1140	-1134	-1134	-66	-1074	-1068	-1068	-1070	3
50	150	38	25	-1120	-1126	-1120	-66	-1054	-1060	-1054	-1056	3
50	150	38	30	-1141	-1148	-1148	-66	-1075	-1082	-1082	-1080	4
50	150	38	40	-1164	-1170	-1164	-66	-1098	-1104	-1098	-1100	3
50	150	38	50	-1166	-1171	-1167	-66	-1100	-1105	-1101	-1102	3
50	150	38	60	-1169	-1175	-1172	-67	-1102	-1108	-1105	-1105	3
			$KMnO_4$									
50	150	38	25	-1266	-1273	-1271	-67	-1199	-1206	-1204	-1203	4
50	150	38	37.5	-1091	-1097	-1097	-68	-1023	-1029	-1029	-1027	3
50	150	38	50	-1080	-1085	-1084	-68	-1012	-1017	-1016	-1015	3
50	150	38	75	-1142	-1149	-1147	-69	-1073	-1080	-1078	-1077	4
50	150	38	100	-1139	-1145	-1142	-71	-1068	-1074	-1071	-1071	3

Appendix C. Solution resistance measurements

[Zn]	$[H_2SO_4]$	Temperature	Additive	Solution resistance (Rs)				
				Ω				
(gL^{-1})		(^0C)	(mgL^{-1})	1	2	3	Mean	Standard deviation
10	150	38	None	0.812	0.814	0.813	0.813	0.001
30	150	38	None	0.921	0.925	0.915	0.920	0.005
40	150	38	None	0.987	0.993	0.995	0.992	0.004
60	150	38	None	1.056	1.059	1.062	1.059	0.003
80	150	38	None	1.084	1.079	1.075	1.079	0.005
90	150	38	None	1.234	1.229	1.231	1.231	0.003
100	150	38	None	1.316	1.307	1.315	1.313	0.005
120	150	38	None	1.443	1.449	1.439	1.444	0.005
50	0	38	None	9.057	9.064	9.062	9.061	0.004
50	10	38	None	6.235	6.229	6.24	6.235	0.006
50	50	38	None	2.618	2.612	2.614	2.615	0.003
50	100	38	None	1.405	1.406	1.399	1.403	0.004
50	200	38	None	0.873	0.869	0.875	0.872	0.003
50	250	38	None	0.763	0.758	0.762	0.761	0.003
50	150	20	None	1.183	1.179	1.178	1.180	0.003
50	150	30	None	1.091	1.094	1.089	1.091	0.003
50	150	40	None	1.074	1.069	1.068	1.070	0.003
50	150	50	None	0.91	0.904	0.899	0.904	0.006
50	150	60	None	0.804	0.797	0.803	0.801	0.004
50	150	70	None	0.691	0.701	0.697	0.696	0.005
			TBABr					
50	150	38	2	0.953	0.948	0.954	0.951	0.003
50	150	38	5	0.947	0.951	0.953	0.949	0.003
50	150	38	10	0.952	0.948	0.954	0.950	0.003
50	150	38	40	0.955	0.956	0.961	0.956	0.003
50	150	38	100	0.967	0.968	0.972	0.968	0.003

Appendix C. Continued

[Zn]	$[H_2SO_4]$	Temperature	Additive	Solution resistance (Rs) Ω				
(gL^{-1})		(^0C)	(mgL^{-1})	1	2	3	Mean	Standard deviation
			Saccharin					
50	150	38	2.5	0.95	0.953	0.947	0.950	0.003
50	150	38	5	0.948	0.953	0.952	0.951	0.003
50	150	38	15	0.954	0.949	0.956	0.953	0.004
50	150	38	25	0.958	0.952	0.954	0.955	0.003
50	150	38	40	0.949	0.954	0.952	0.952	0.003
50	150	38	60	0.954	0.948	0.952	0.951	0.003
50	150	38	80	0.961	0.956	0.955	0.957	0.003
50	150	38	100	0.978	0.982	0.983	0.981	0.003
			Pyridine					
50	150	38	1	0.983	0.978	0.982	0.981	0.003
50	150	38	5	0.976	0.972	0.971	0.973	0.003
50	150	38	10	0.973	0.969	0.974	0.972	0.003
50	150	38	20	0.968	0.972	0.974	0.971	0.003
50	150	38	30	0.961	0.963	0.958	0.961	0.003
50	150	38	40	0.976	0.973	0.97	0.973	0.003
50	150	38	55	0.971	0.976	0.974	0.974	0.003
50	150	38	70	0.967	0.97	0.973	0.970	0.003
50	150	38	85	0.972	0.974	0.969	0.970	0.003
50	150	38	100	0.983	0.979	0.984	0.980	0.003
			Pyridine; Saccharin					
50	150	38	10;100	1.017	1.012	1.014	1.014	0.004
50	150	38	40;40	0.989	0.993	0.996	0.993	0.003

Appendix C. Continued

[Zn]	$[H_2SO_4]$	Temperature	Additive	Solution resistance (Rs) Ω				
(gL^{-1})		(^0C)	(mgL^{-1})	1	2	3	Mean	Standard deviation
			Butyne-1,4,diol					
50	150	38	1	0.981	0.979	0.985	0.980	0.003
50	150	38	3.5	0.986	0.981	0.98	0.984	0.003
50	150	38	5	0.992	0.993	0.988	0.993	0.003
50	150	38	10	0.998	0.991	0.991	0.995	0.004
50	150	38	15	0.973	0.974	0.969	0.974	0.003
50	150	38	20	0.982	0.979	0.985	0.981	0.003
50	150	38	25	0.985	0.981	0.979	0.983	0.003
50	150	38	30	0.981	0.987	0.983	0.984	0.003
50	150	38	40	0.974	0.971	0.968	0.973	0.003
50	150	38	50	0.98	0.982	0.987	0.981	0.004
50	150	38	60	0.983	0.98	0.975	0.982	0.004
			$KMnO_4$					
50	150	38	25	0.991	0.996	0.995	0.994	0.004
50	150	38	37.5	1.001	1.007	1.012	1.007	0.004
50	150	38	50	1.005	1.012	1.006	1.008	0.005
50	150	38	75	1.019	1.024	1.016	1.020	0.004
50	150	38	100	1.039	1.045	1.043	1.042	0.004

Appendix D. Results for frequency response analysis experiments for the different electrolytes.

[Zn]	[H_2SO_4]	Temp	Additive	Rs	(IRs)	Measured Ep	IRs as % of measured Ep	En	Ep	ΔE
(gL^{-1})		(^0C)	(mgL^{-1})	(Ω)	(mV)	(mV vs. SCE)	(%)	(mV vs. SCE)		(mV)
10	150	38	None	0.81	-55	-1169	5	-1104	-1114	10
30	150	38	None	0.92	-62	-1133	6	-1090	-1071	-19
40	150	38	None	0.99	-67	-1131	6	-1078	-1064	-14
60	150	38	None	1.06	-72	-1117	6	-1089	-1045	-44
80	150	38	None	1.08	-73	-1105	7	-1075	-1032	-43
90	150	38	None	1.23	-83	-1100	8	-1035	-1017	-18
100	150	38	None	1.3	-88	-1143	8	-1050	-1055	5
120	150	38	None	1.44	-98	-1134	9	-1033	-1036	3
50	0	38	None	9.06	-614	-1605	38	-1055	-991	-64
50	10	38	None	6.23	-422	-1375	31	-1092	-953	-139
50	50	38	None	2.59	-176	-1243	14	-1080	-1067	-13
50	100	38	None	1.4	-95	-1129	8	-1075	-1034	-41
50	200	38	None	0.87	-59	-1079	5	-1091	-1020	-71
50	250	38	None	0.76	-52	-1069	5	-1083	-1017	-66
50	150	20	None	1.18	-80	-1179	7	-1103	-1099	-4
50	150	30	None	1.09	-74	-1169	6	-1092	-1095	3
50	150	40	None	1.07	-73	-1088	7	-1057	-1015	-42
50	150	50	None	0.9	-61	-1073	6	-1006	-1012	6
50	150	60	None	0.8	-54	-1058	5	-1004	-1004	0
50	150	70	None	0.7	-47	-1052	5	-996	-1005	9

Appendix D. Continued

[Zn]	[H_2SO_4]	Temp	Additive	Rs	(IRs)	Measured Ep	IRs as % of measured Ep	En	Ep	ΔE
(gL^{-1})		(^0C)	(mgL^{-1})	(Ω)	(mV)	(mV vs. SCE)	(%)	(mV vs. SCE)		(mV)
			TBABr							
50	150	38	2	0.95	-64	-1094	6	-1048	-1030	-18
50	150	38	5	0.95	-64	-1106	6	-1045	-1042	-3
50	150	38	10	0.95	-64	-1146	6	-1093	-1082	-11
50	150	38	40	0.96	-65	-1143	6	-1081	-1078	-3
50	150	38	100	0.97	-66	-1149	6	-1100	-1083	-17

Appendix D. Continued

[Zn]	[H_2SO_4]	Temp	Additive	Rs	(IRs)	Measured Ep	IRs as % of measured Ep	En	Ep	ΔE
(gL^{-1})		(^0C)	(mgL^{-1})	(Ω)	(mV)	(mV vs. SCE)	(%)	(mV vs. SCE)		(mV)
			Butyne-1,4, diol							
50	150	38	1	0.98	-66	-1196	6	-1139	-1130	-9
50	150	38	3.5	0.98	-66	-1191	6	-1135	-1125	-10
50	150	38	5	0.99	-67	-1186	6	-1132	-1119	-13
50	150	38	10	0.99	-67	-1174	6	-1136	-1107	-29
50	150	38	15	0.97	-66	-1152	6	-1134	-1086	-48
50	150	38	20	0.98	-66	-1136	6	-1120	-1070	-50
50	150	38	25	0.98	-66	-1122	6	-1110	-1056	-54
50	150	38	30	0.98	-66	-1144	6	-1135	-1078	-57
50	150	38	40	0.97	-66	-1166	6	-1141	-1100	-41
50	150	38	50	0.98	-66	-1168	6	-1129	-1102	-27
50	150	38	60	0.99	-67	-1172	6	-1120	-1105	-15
			Pyridine; Saccharin							
50	150	38	10;100	1.01	-68	-1224	6	-1187	-1156	-31
50	150	38	40;40	0.99	-67	-1252	5	-1151	-1185	-34

Appendix D. Continued

[Zn]	$[H_2SO_4]$	Temp	Additive	Rs	(IRs)	Measured Ep	IRs as % of measured Ep	En	Ep	ΔE
(gL^{-1})		(^0C)	(mgL^{-1}) $KMnO_4$	(Ω)	(mV)	(mV vs. SCE)	(%)	(mV vs. SCE)		(mV)
50	150	38	25	0.99	-67	-1270	5	-1138	-1203	65
50	150	38	37.5	1	-68	-1095	6	-1063	-1027	-36
50	150	38	50	1	-68	-1083	6	-1057	-1015	-42
50	150	38	75	1.02	-69	-1146	6	-1044	-1077	33
50	150	38	100	1.04	-71	-1142	6	-1064	-1071	7

Appendix E. Calculation of current efficiency

Current Efficiency (CE) = (Mass of zinc plated/Theoretical mass) x 100%. 8.1

Theoretical mass, m, (g) plated for 80minutes at a constant current of 0.068A is given by

m = ItAr/nF 8.2

Where:

I (A) is the current passing through the electrolyte, t (s) is the plating time, Ar (g/mole) is the relative atomic mass, n (mole e^-/mole deposited zinc) and F (C/mole electrons) is Faraday's constant.

= (0.068A) x 4800s (65)/2 x (96485)
= 0.1099g

Appendix F. Measurements of plated mass

[Zn] (gL^{-1})	[H_2SO_4] (gL^{-1})	Temperature (^0C)	Additive (mgL^{-1})	Mass plated (g)					
				1	2	3	mean	Standard deviation	Current efficiency (%)
10	150	38	None	0.069	0.070	0.071	0.070	0.001	63
30	150	38	None	0.109	0.107	0.108	0.108	0.001	98
40	150	38	None	0.108	0.110	0.108	0.108	0.001	99
60	150	38	None	0.110	0.108	0.110	0.109	0.001	99
80	150	38	None	0.109	0.108	0.110	0.109	0.001	99
90	150	38	None	0.084	0.082	0.087	0.084	0.003	77
100	150	38	None	0.082	0.085	0.086	0.085	0.002	77
120	150	38	None	0.081	0.083	0.081	0.082	0.001	74
50	0	38	None	0.069	0.068	0.067	0.068	0.001	62
50	10	38	None	0.079	0.082	0.080	0.081	0.002	73
50	50	38	None	0.085	0.087	0.082	0.084	0.002	77
50	100	38	None	0.090	0.091	0.089	0.090	0.001	82
50	200	38	None	0.092	0.093	0.091	0.092	0.001	84
50	250	38	None	0.109	0.105	0.107	0.107	0.002	97
50	150	20	None	0.087	0.089	0.090	0.089	0.001	81
50	150	30	None	0.091	0.090	0.092	0.091	0.001	83
50	150	40	None	0.108	0.110	0.107	0.108	0.002	98
50	150	50	None	0.070	0.068	0.067	0.068	0.002	62
50	150	60	None	0.051	0.048	0.050	0.050	0.002	45
50	150	70	None	0.033	0.032	0.035	0.033	0.001	30

Appendix F. Continued

[Zn]	$[H_2SO_4]$	Temperature	Additive	Mass plated					
(gL^{-1})		(^0C)	(mgL^{-1})	(g)					(%)
				1	2	3	mean	Standard deviation	Current efficiency
			TBABr						
50	150	38	2	0.096	0.095	0.098	0.096	0.002	87
50	150	38	5	0.099	0.100	0.101	0.100	0.001	91
50	150	38	10	0.094	0.095	0.096	0.095	0.001	86
50	150	38	40	0.096	0.096	0.093	0.095	0.001	86
50	150	38	100	0.088	0.090	0.087	0.088	0.001	80
			Saccharin						
50	150	38	2.5	0.084	0.084	0.081	0.083	0.002	75
50	150	38	5	0.075	0.074	0.077	0.075	0.002	68
50	150	38	15	0.096	0.095	0.096	0.096	0.001	87
50	150	38	25	0.080	0.078	0.080	0.079	0.001	72
50	150	38	40	0.065	0.067	0.066	0.066	0.001	60
50	150	38	60	0.060	0.061	0.062	0.061	0.001	55
50	150	38	80	0.045	0.042	0.044	0.044	0.002	40
50	150	38	100	0.035	0.034	0.033	0.034	0.001	31

Appendix F. Continued

[Zn]	$[H_2SO_4]$	Temperature	Additive	Mass plated					
(gL^{-1})		(^0C)	(mgL^{-1})	(g)					(%)
				1	2	3	mean	Standard deviation	Current efficiency
			Pyridine						
50	150	38	1	0.076	0.079	0.076	0.077	0.002	70
50	150	38	5	0.071	0.073	0.073	0.072	0.001	66
50	150	38	10	0.076	0.079	0.077	0.077	0.001	70
50	150	38	20	0.071	0.073	0.074	0.073	0.002	66
50	150	38	30	0.073	0.075	0.072	0.073	0.001	67
50	150	38	40	0.076	0.074	0.075	0.075	0.001	68
50	150	38	55	0.075	0.073	0.075	0.074	0.001	67
50	150	38	70	0.077	0.076	0.074	0.076	0.002	69
50	150	38	85	0.070	0.072	0.067	0.070	0.002	63
50	150	38	100	0.066	0.065	0.067	0.066	0.001	60
			Pyridine; Saccharin						
50	150	38	10;100	0.032	0.028	0.029	0.029	0.002	27
50	150	38	40;40	0.041	0.039	0.037	0.039	0.002	36

Appendix F. Continued.

[Zn]	[H_2SO_4]	Temperature	Additive	Mass plated					
(gL^{-1})		(^0C)	(mgL^{-1})	(g)					(%)
				1	2	3	mean	Standard deviation	Current efficiency
			Butyne-1,4,diol						
50	150	38	1	0.083	0.083	0.085	0.083	0.001	76
50	150	38	3.5	0.083	0.084	0.081	0.083	0.002	76
50	150	38	5	0.086	0.084	0.086	0.085	0.001	77
50	150	38	10	0.082	0.084	0.085	0.084	0.002	76
50	150	38	15	0.083	0.085	0.080	0.083	0.002	75
50	150	38	20	0.085	0.085	0.080	0.083	0.003	76
50	150	38	25	0.078	0.082	0.082	0.081	0.002	74
50	150	38	30	0.085	0.085	0.081	0.084	0.002	76
50	150	38	40	0.087	0.088	0.084	0.086	0.002	78
50	150	38	50	0.087	0.084	0.084	0.085	0.001	77
50	150	38	60	0.082	0.085	0.085	0.084	0.002	76
			$KMnO_4$						
50	150	38	25	0.087	0.085	0.087	0.086	0.001	78
50	150	38	37.5	0.087	0.085	0.087	0.087	0.001	79
50	150	38	50	0.089	0.090	0.089	0.089	0.001	81
50	150	38	75	0.090	0.092	0.091	0.091	0.001	83
50	150	38	100	0.084	0.085	0.086	0.085	0.001	77